applied sciences

MDPI

Article

Fatigue Life Prediction of Steels in Hydrogen Environments Using Physics-Informed Learning

Huaxi Wu [1], Xinkai Guo [2], Wen Sun [2], Lu-Kai Song [2,3], Qingyang Deng [4,5], Shiyuan Yang [6,*] and Debiao Meng [1,2,*]

[1] School of Mechanical and Electrical Engineering, University of Electronic Science and Technology of China, Chengdu 611731, China; 202522040453@std.uestc.edu.cn
[2] Institute of Electronic and Information Engineering of UESTC in Guangdong, Dongguan 523808, China; smtgxk@126.com (X.G.); dyysunwen@126.com (W.S.); slk@ustb.edu.cn (L.-K.S.)
[3] School of Mechanical Engineering, University Science and Technology Beijing, Beijing 100083, China
[4] Faculty of Geosciences and Engineering, Southwest Jiaotong University, Chengdu 611756, China; dqy@my.swjtu.edu.cn
[5] College of Engineering Architecture Technology, Oklahoma State University, Stillwater, OK 74075, USA
[6] LAETA, Faculdade de Engenharia, Universidade do Porto, Rua Dr. Roberto Frias, 4200-425 Porto, Portugal
* Correspondence: up202311575@edu.fe.up.pt (S.Y.); dbmeng@uestc.edu.cn (D.M.)

Abstract

Hydrogen embrittlement poses a critical threat to the durability of metallic components in emerging hydrogen energy infrastructure. Reliable fatigue life assessment in hydrogen-rich environments is, however, severely constrained by the high cost and low throughput of high-pressure testing, resulting in characteristically sparse experimental datasets. Conventional empirical fatigue models struggle to capture hydrogen–mechanical coupling effects, while purely data-driven approaches often suffer from severe overfitting under data-scarce conditions. To address this challenge, this study develops a physics-enhanced learning framework that integrates established fracture mechanics principles with machine learning. Using high-strength GS80A steel as a case study, two complementary strategies are introduced. First, a physically augmented input strategy reformulates raw experimental variables into dimensionless physical descriptors derived from the Basquin and Goodman relations, thereby reducing the complexity of the learning space. Second, a physics-regularized ensemble strategy combines deterministic physical predictions with neural network outputs through a dual-pathway inference scheme, ensuring physically admissible behavior during extrapolation. An automated hyperparameter selection module is further employed to establish a robust data-driven baseline. Comparative evaluation against optimized multi-layer perceptron and support vector regression models demonstrates that the proposed framework significantly improves predictive robustness in small-sample regimes. Specifically, the coefficient of determination (R^2) exceeds 0.975, with the root mean square error (RMSE) reduced by approximately 70% compared to the pure data-driven baseline. By systematically embedding mechanistic priors into the learning process, the proposed approach provides a reliable and interpretable tool for fatigue assessment of metallic components operating in hydrogen environments.

Keywords: hydrogen embrittlement; fatigue life assessment; physics-enhanced learning; fracture mechanics; sparse experimental data

Check for updates

Received: 12 January 2026
Revised: 11 February 2026
Accepted: 11 February 2026
Published: 13 February 2026

Copyright: © 2026 by the authors. Licensee MDPI, Basel, Switzerland. This article is an open access article distributed under the terms and conditions of the Creative Commons Attribution (CC BY) license.

1. Introduction

The accelerating global transition towards a decarbonized energy paradigm has established hydrogen as a pivotal vector for achieving carbon neutrality targets across industrial and transportation sectors [1]. As nations aggressively expand hydrogen infrastructure, encompassing high-pressure transmission pipelines, storage vessels, and refueling stations, the compatibility of metallic materials with high-pressure hydrogen gas has emerged as a critical bottleneck limiting safe and economic deployment [2]. The interaction between structural steels and atomic hydrogen precipitates a catastrophic degradation mechanism known as Hydrogen Embrittlement. This phenomenon fundamentally alters the mechanical response of the material lattice, transforming ductile failure modes into unpredictable brittle fractures and drastically reducing fatigue life [3,4]. Consequently, the development of robust, accurate methodologies for assessing the structural integrity of components exposed to hydrogen is not merely an engineering prerequisite but a fundamental safety mandate for the nascent hydrogen economy [5].

Assessing the fatigue life of metals in hydrogen-rich environments presents a distinct set of phenomenological and logistical challenges compared to testing in inert atmospheres [6]. The fatigue process under hydrogen exposure is governed by a complex, multi-scale interaction between cyclic mechanical loading and hydrogen diffusion kinetics [7]. Mechanisms such as Hydrogen Enhanced Decohesion and Hydrogen Enhanced Local Plasticity operate synergistically to accelerate crack initiation and propagation, introducing severe non-linearities into the material response [8,9]. Quantifying this degradation typically requires conducting fatigue tests in high-pressure autoclaves, a process that is technologically demanding, hazardous, and exorbitantly expensive [10]. Unlike standard air fatigue tests where high-frequency resonance machines can rapidly generate extensive datasets, hydrogen fatigue testing is inherently limited to low frequencies to allow sufficient time for diffusion-controlled damage accumulation [11]. This constraint results in a systemic scarcity of high-fidelity experimental data. The resultant small sample regime poses a significant barrier to reliability assessment, as engineers are frequently forced to extrapolate long-term service life from a sparse, heteroscedastic set of experimental observations [12,13].

Fatigue life prediction for engineering components has traditionally relied on two primary methodological pillars: phenomenological statistical models and fracture mechanics approaches [14,15]. Empirical methods, such as the Basquin stress-life formulation and the Goodman mean stress correction, characterize total fatigue life through power-law relationships derived from extensive experimental fitting [16–18]. While these phenomenological models provide a deterministic baseline for design in benign environments, they are fundamentally empirical and lack the intrinsic flexibility to account for the complex environmental coupling effects introduced by hydrogen [19]. Conversely, fracture mechanics approaches focus on crack propagation kinetics [20], but depend heavily on the precise determination of threshold stress intensity factors, which exhibit significant stochasticity in hydrogen environments due to local trapping effects [21]. Both paradigms struggle to generalize across the diverse operating conditions encountered in service, often leading to designs that are either overly conservative or susceptible to unexpected failure [22,23]. As noted in the comprehensive review by Barrera et al. [24], traditional fracture mechanics models often fail to adapt to the highly non-linear synergistic effects of hydrogen concentration gradients and plasticity evolution. Consequently, both paradigms struggle to generalize across the diverse operating conditions encountered in service, often leading to designs that are either overly conservative or susceptible to unexpected failure.

The advent of Industry 4.0 and the exponential growth in computational power have recently catalyzed a paradigm shift towards data-driven modeling [25]. Machine learn-

ing algorithms, particularly Artificial Neural Networks, have demonstrated remarkable efficacy in capturing complex, non-linear patterns that elude traditional analytical formulations [26–31]. In the context of material science, these data-driven approaches offer the potential to map the intricate relationship between loading parameters, environmental variables, and fatigue life without relying on rigid preconceived physical assumptions [31,32]. By treating the material response as a high-dimensional regression problem, neural networks can theoretically uncover latent correlations between electrochemical charging conditions and mechanical degradation [33].

Nevertheless, the application of pure data-driven intelligence to hydrogen fatigue prediction is fraught with epistemic risks. The fundamental premise of deep learning is the availability of massive, representative datasets that allow the network to inductively learn the underlying manifold of the system [34–37]. In the domain of hydrogen embrittlement, where data is inherently sparse, pure machine learning models are prone to severe overfitting. As highlighted by Yuan et al. [38], without physical constraints, these unconstrained algorithms tend to memorize experimental noise rather than learning physical laws, resulting in thermodynamic inadmissibility during extrapolation. A standard Multi-Layer Perceptron trained on a limited dataset may achieve negligible error on training points but produce thermodynamically inadmissible predictions when extrapolating to unseen regimes [39–41]. For instance, a purely statistical model might paradoxically predict an increase in fatigue life with increasing stress amplitude simply because it has memorized the noise in the training data rather than the physical signal [42]. Furthermore, the opaque nature of these black-box algorithms hinders their adoption in safety-critical industries, where interpretability and adherence to physical laws are non-negotiable requirements for certification and risk management [43,44].

To reconcile the asymptotic robustness of physical laws with the non-linear flexibility of data-driven methods, the emerging field of Physics-Informed Machine Learning represents a promising frontier [45,46]. By embedding domain knowledge directly into the learning architecture, these hybrid models constrain the search space of the neural network, ensuring that predictions remain physically consistent even in data-scarce scenarios [47,48]. While Physics-Informed Neural Networks have achieved notable success in solving partial differential equations for fluid dynamics and heat transfer, their direct application to fatigue life assessment remains challenging due to the discrete and highly scattered nature of fatigue data [49]. Unlike conventional physics-informed approaches that embed differential equation residuals directly into the loss function, the framework proposed in this study adopts a distinct hybrid strategy tailored for data scarcity. It integrates phenomenological fatigue laws as geometric constraints within the feature space and as regularization terms at the decision level. This approach effectively formulates the empirical laws of fatigue as differentiable constraints that guide the network optimization [50,51], thereby balancing the inductive bias of physical priors with the flexibility required to learn environmental deviations.

To address these limitations, this study proposes a novel Physics Enhanced Learning Framework (PELF) designed specifically for the fatigue life assessment of structural steels in hydrogen environments. Unlike binary choices between analytical equations and black-box algorithms, this framework establishes a gray-box architecture that synergizes mechanistic priors with data-driven computation. The primary contributions of this work are threefold:

- Optimization of the Data-Driven Baseline: We introduce an Automated Hyperparameter Selection Module (AHSM) to dynamically refine network topology, ensuring optimal generalization capabilities prior to physical integration.

- Physical Feature Augmentation: A Physically Augmented Input Strategy (PAIS) is developed, which linearizes the learning manifold by transforming raw inputs into dimensionless physical descriptors derived from Basquin and Goodman relations.
- Hybrid Model Regularization: We propose a Physics Regularized Ensemble Strategy (PRES) that fuses deterministic physical outputs with neural network predictions. This dual-pathway mechanism allows the model to maintain high accuracy in data-rich regions while promoting adherence to physical trends during extrapolation. Through a comprehensive comparative analysis against conventional MLP and SVR models, this study demonstrates that embedding physical constraints significantly reduces prediction error in small-sample regimes and improves the generalization potential when extending predictions from low-pressure to high-pressure environments.

The efficacy of the proposed framework is validated using experimental datasets for GS80A steel, a critical material for offshore infrastructure. Through a comprehensive comparative analysis against conventional MLP (Multi-Layer Perceptron) and SVR (Support Vector Regression) models, this study demonstrates that embedding physical constraints significantly reduces prediction error in small-sample regimes and enables robust extrapolation from low-pressure to high-pressure environments. The remainder of this manuscript is organized as follows: Section 2 establishes the theoretical foundations of hydrogen fatigue and the statistical baselines. Section 3 articulates the architecture of the proposed Physics Enhanced Learning Framework, detailing the AHSM, PAIS, and PRES modules. Section 4 presents experimental validation using GS80A steel and discusses the comparative analysis results. Finally, Section 5 concludes the study and outlines future research directions.

2. Theoretical Preliminaries

2.1. Fatigue Mechanisms in Hydrogen Environments

The fatigue failure of high-strength structural steels in high-pressure hydrogen environments is governed by a stochastic interplay between cyclic mechanical damage and electrochemical hydrogen uptake [52]. Unlike fatigue in inert media where damage accumulation is dominated by surface slip-band intrusion and extrusion, the ingress of atomic hydrogen fundamentally alters the micromechanical response of the crystal lattice. Current phenomenological understanding attributes this degradation primarily to the synergistic action of Hydrogen Enhanced Decohesion and Hydrogen Enhanced Local Plasticity [53].

The Hydrogen Enhanced Decohesion mechanism postulates that interstitial hydrogen accumulates in regions of high hydrostatic stress, specifically at crack tips and grain boundaries, thereby lowering the cohesive bond strength of the metal lattice [54]. This reduction in theoretical fracture stress precipitates a transition from ductile striation formation to brittle intergranular cleavage, particularly in the high-stress, low-cycle fatigue regime [55]. Concurrently, the Hydrogen Enhanced Local Plasticity mechanism suggests that hydrogen atmospheres shield the elastic stress fields surrounding dislocations, reducing the activation energy required for dislocation mobility. This phenomenon induces highly localized plastic deformation within microscopic volumes, promoting premature micro-void coalescence even while the macroscopic bulk behavior exhibits reduced ductility [56].

In practical service conditions, the dominance of either mechanism is contingent upon the local hydrogen concentration, loading frequency, and the stress intensity factor range [57]. This mechanistic complexity introduces severe non-linearities and heteroscedasticity into the fatigue life distribution, rendering traditional deterministic models insufficient for capturing the full spectrum of degradation. Consequently, accurate life prediction necessitates a modeling paradigm that can reconcile macroscopic governing laws with the underlying mechanistic stochasticity induced by hydrogen diffusion [58]. In the proposed

framework, the synergistic action of HELP and HEDE mechanisms, specifically the scatter in fatigue life induced by local hydrogen accumulation, is treated as an intrinsic source of aleatoric uncertainty. By design, the data-driven pathway of the model is tasked with capturing this specific stochastic deviation, thereby establishing a direct link between the qualitative micromechanical mechanisms and the quantitative predictive architecture.

2.2. Governing Equations for Fatigue Life

To regularize the learning process of the neural networks, established constitutive relations of fatigue analysis are invoked. It is important to clarify that while formulations such as the Basquin and Goodman relations are fundamental to engineering design, they represent phenomenological boundaries of material behavior derived from empirical fitting rather than strict mechanistic derivations from first-principle fracture mechanics. For total fatigue life prediction in the high-cycle regime where elastic deformation dominates, the relationship between the applied stress amplitude σ_a and the number of reversals to failure $2N_f$ is governed by the Basquin constitutive relation. In its linearized logarithmic form, which provides the canonical basis for S-N curve analysis, the equation is expressed as

$$\log(\sigma_a) = \log\left(\sigma_{f'}\right) + b \cdot \log\left(2N_f\right) \tag{1}$$

where $\sigma_{f'}$ denotes the fatigue strength coefficient and b represents the fatigue strength exponent. While hydrogen embrittlement inevitably degrades these material constants by shifting the S-N curve downwards and altering its slope, the power-law functional form remains a robust first-order approximation of the damage accumulation process.

Engineering components typically operate under non-zero mean stress conditions. The presence of tensile mean stress σ_m is critical in hydrogen environments as it facilitates hydrogen diffusion into the fracture process zone through hydrostatic stress gradients [59]. The Goodman relation is employed to correct the fatigue limit by coupling the alternating stress with the Ultimate Tensile Strength S_u of the material:

$$\frac{\sigma_a}{S_{N_f}} + \frac{\sigma_m}{S_u} = 1 \tag{2}$$

Rearranging this formulation allows for the derivation of an equivalent fully reversed stress amplitude, or theoretically, a predicted fatigue limit S_{N_f} for a specific lifetime. This derivation transforms the independent variables into a unified physical descriptor ξ:

$$S_{N_f} = \frac{\sigma_a}{1 - \frac{\sigma_m}{S_u}} \tag{3}$$

Regarding the fatigue crack growth rate, which constitutes the propagation phase of fatigue life, the kinetics are described by the Paris–Erdogan law. The relationship between the crack growth rate $\frac{da}{dN}$ and the stress intensity factor range ΔK follows a power law. In hydrogen environments, the coefficient C and exponent m become highly sensitive to hydrogen pressure and frequency [60]. The logarithm of this law serves as the physical regularization term in the loss function of the proposed framework, constraining the network to adhere to fracture mechanics principles even when extrapolating data from low-pressure to high-pressure regimes:

$$\log\left(\frac{da}{dN}\right) = \log(C) + m\log(\Delta K) \tag{4}$$

The logarithm of this law serves as the physical regularization term in the loss function of the proposed framework. Specifically, the deviation between the neural network

gradient output and the theoretical crack growth rate defined by the Paris law is computed as a penalty term. This constrains the optimization landscape, forcing the model to adhere to valid fracture mechanics principles, specifically the monotonic increase in crack growth rate with stress intensity, even when extrapolating data from low-pressure to high-pressure regimes.

2.3. Machine Learning Baselines

The Multi-Layer Perceptron serves as a universal approximator to map the input feature space to the target fatigue life [61]. Rather than relying on generic default configurations, this study implements a rigorous hyperparameter optimization scheme, the details of which are provided in Section 3.2.1, to determine the optimal number of hidden layers and neurons. Despite their expressiveness, MLPs lack epistemic awareness of physical constraints. In small-sample regimes characteristic of hydrogen fatigue testing, unconstrained networks often produce physically inconsistent predictions in the extrapolation domain, such as violating the fundamental inverse relationship between stress amplitude and fatigue life.

Conversely, Support Vector Regression addresses the generalization problem through the principle of Structural Risk Minimization [62]. By mapping input data into a high-dimensional feature space via a kernel function, SVR seeks a linear regression hyperplane that minimizes the norm of the weights subject to epsilon-insensitive tube constraints. While offering superior robustness for small datasets compared to standard neural networks, SVR remains a purely statistical method that treats fatigue life prediction as a generic regression task, ignoring the specific constitutive priors defined by the Basquin and Goodman relations.

3. The Proposed Physics Informed Framework

3.1. Framework Architecture for Data Scarce Scenarios

Accurate fatigue life prediction in hydrogen environments is inherently constrained by the sparsity of high-fidelity experimental data, a consequence of the prohibitive costs and temporal demands of hydrogen charged testing. While conventional data-driven approaches, such as standalone Artificial Neural Networks, excel in feature extraction, they are prone to overfitting in small sample regimes, often failing to satisfy physical consistency constraints. Conversely, classical empirical models such as the Basquin model and Paris' law, though robust, lack the flexibility required to capture the intricate, nonlinear coupling effects induced by hydrogen embrittlement.

To reconcile these limitations, this study proposes the Physics Enhanced Learning Framework (PELF). Diverging from traditional black box paradigms, the PELF operates as a gray box system, systematically embedding domain knowledge to regularize the learning process. The architecture is predicated on the synergy of three functional modules:

Automated Hyperparameter Selection Module (AHSM): To mitigate the bias and inefficiency inherent in manual tuning, the framework incorporates an adaptive optimization engine. By integrating rigorous cross validation with grid search algorithms, the AHSM dynamically refines the network topology and regularization parameters. This ensures that the baseline statistical model achieves optimal generalization capabilities prior to physical integration, thereby establishing a robust data driven foundation.

Physical Prior Knowledge Block: This component acts as the theoretical anchor, encapsulating governing phenomenological fatigue laws, specifically the Basquin equation and Goodman's mean stress correction. Unlike strict fracture mechanics derivations, these empirical priors provide a first-order approximation of the material response. By embedding these relationships, the block supplies deductive constraints that regularize the learning

process, guiding the model's baseline behavior to align with established engineering trends rather than guaranteeing absolute physical compliance.

Dual Pathway Integration Interface: The framework employs a hybrid integration strategy detailed in Section 3.2.3. (1) Input Level Augmentation (PAIS): Physical priors are mapped into dimensionless descriptors to reduce feature space complexity. (2) Output Level Regularization (PRES): A dynamic ensemble mechanism fuses analytical outputs with machine learning inference. This dual-pathway approach promotes adherence to physical consistency while retaining the flexibility to model local nonlinearities associated with hydrogen degradation.

3.2. Fusing Physical Priors with Data Driven Models

3.2.1. The Optimized Baseline Module

Prior to integrating physical constraints, it is imperative to establish a rigorous data driven baseline capable of capturing the inherent nonlinearities in the fatigue data. To this end, two distinct machine learning architectures were employed as the backbone of the framework: the Multi-Layer Perceptron MLP and SVR. The MLP was selected for its universal approximation capabilities, while SVR was included for its proven robustness in small sample regimes through the principle of structural risk minimization. However, the performance of these models is heavily contingent upon the precise calibration of their hyperparameters. Manual tuning in such high dimensional parameter spaces is not only inefficient but also susceptible to researcher bias and overfitting, particularly when data is scarce. To resolve this, this study implements an AHSM driven by an exhaustive Grid Search coupled with K fold Cross Validation.

The optimization process is formulated as follows: Let H represent the hyperparameter space. The objective is to identify the optimal configuration vector $\theta^* \in H$ that minimizes the generalization error. To ensure the statistical reliability of the performance evaluation, a 5-fold cross validation strategy is adopted. The training dataset D is randomly partitioned into $k = 5$ disjoint subsets $\{D_1, \ldots, D_k\}$. For each candidate configuration θ, the model is trained on $k - 1$ subsets and validated on the remaining subset. This process is iterated k times, and the final performance metric $E(\theta)$ is calculated as the average validation error:

$$E(\theta) = \frac{1}{k}\sum_{i=1}^{k}\left(\frac{1}{|D_i|}\sum_{j=1}^{|D_i|}(y_i - \hat{y}_j)^2\right) \tag{5}$$

where the inner term represents the Mean Squared Error (MSE) computed on the validation subset D_i. To eliminate variability arising from random partitioning and ensure strict reproducibility, the random seed for the K-fold split is fixed to a constant value (Seed = 42) across all experimental runs.

Within this framework, the search space for the MLP architecture includes variations in number of hidden layers and neurons, activation functions and optimization solvers. Conversely, for the SVR architecture, the optimization targets the kernel function type, the regularization parameter C, and the epsilon insensitive tube width ε. By systematically traversing these parameter grids, the AHSM identifies the optimal candidate configuration within the explored search space, providing a solid, unbiased foundation for the subsequent integration of physical priors. The comprehensive architecture of this automated optimization framework is systematically depicted in Figure 1.

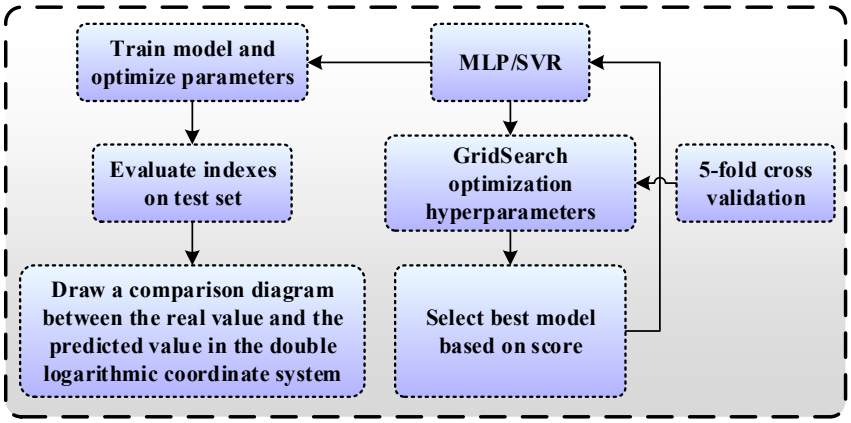


Figure 1. Schematic workflow of the Automated Hyperparameter Selection Module for optimizing the data driven baseline.

3.2.2. Strategy I: Feature Engineering via Physical Relations

While the optimized baseline module establishes a statistical foundation for fatigue life prediction, its efficacy is inherently bounded by the representational density of the training data. In high dimensional feature spaces, purely data driven models such as the MLP require substantial volumes of data to implicitly reconstruct the governing manifolds of material behavior. When training data is scarce, as is the case with hydrogen charged fatigue testing, the network struggles to distinguish between the true underlying physical laws and stochastic noise, leading to poor extrapolation capabilities. To mitigate this fundamental limitation, the first strategy proposed in this framework, termed the Physically Augmented Input Strategy (PAIS), integrates established fracture mechanics theories directly into the feature space. This approach is predicated on the hypothesis that assisting the neural network with precalculated, physically meaningful variables can significantly reduce the complexity of the learning task, effectively transforming the problem from one of unguided function approximation to one of residual correction.

The theoretical underpinning of this strategy is rooted in the classical stress life ($S-N$) methodology, which remains the dominant paradigm for high cycle fatigue analysis. For metallic materials operating in the elastic regime, the relationship between the applied stress amplitude and the number of reversals to failure is governed by the Basquin constitutive relation. This empirical law posits a power law dependency, which serves as the primary physical constraint for the feature engineering process. Mathematically, the Basquin equation is expressed as

$$\sigma_a = \sigma_{f'} \left(2N_f\right)^b \tag{6}$$

The relationship is defined by Equation (1), as previously described in Section 2.2. While this equation provides a robust description of fatigue behavior in inert environments, the presence of hydrogen introduces nonlinear deviations that perturb the material constants. However, the functional form of the equation remains a valid first order approximation of the damage accumulation process.

Furthermore, engineering components are rarely subjected to fully reversed loading cycles in isolation. The influence of mean stress on fatigue life is a critical factor that must be accounted for to ensure the physical fidelity of the model. To address this, the Goodman relation is invoked as a complementary physical prior. The Goodman line provides a simplified yet effective method for correcting the fatigue limit based on the tensile strength and the applied mean stress. The interaction between these mechanical parameters is defined by Equation (2). By rearranging this equation, one can derive a

theoretical expression for the fatigue limit S_{N_f} that implicitly accounts for the loading ratio and material strength. This derivation transforms the raw, independent input variables into a synthesized physical descriptor.

The core innovation of the PAIS architecture lies in the specific transformation of the input vector. In a traditional machine learning setup, the input vector X would typically consist of raw experimental parameters, such as the stress amplitude σ_a, the hydrogen charging condition H_{cond}, and the mean stress σ_m. These variables are mathematically orthogonal to the network, which must infer the complex multiplicative and exponential relationships between them through the optimization of weight matrices. In the proposed PAIS framework, the input space is augmented or in some iterations, replaced by derived features that encapsulate the interactions defined by the Basquin and Goodman equations.

Specifically, a dimensionless interaction term ξ is constructed, defined as the ratio of the theoretical fatigue limit to the applied stress amplitude:

$$\xi = \frac{S_{N_f}}{\sigma_a} \tag{7}$$

The calculation of ξ is performed dynamically for each data point. The theoretical fatigue limit S_{N_f} is derived by substituting the specific material constants ($\sigma\prime_f, b$) and the cycle count N_f into the inverted Basquin equation, strictly following the procedure outlined in Section 4.3.3.

This engineered feature ξ compresses the information regarding load severity, mean stress effect, and material strength into a single scalar value that holds direct physical significance. Intuitively, this ratio reflects the safety margin or the proximity of the current loading state to the theoretical failure boundary. When ξ is high, the material is operating well within its fatigue limits; when ξ approaches unity, failure is imminent. By feeding this derived feature into the neural network, the model is relieved of the burden of learning the fundamental stress life interaction from scratch. Instead, the AHSM can focus its computational capacity on mapping how the hydrogen environment perturbs this fundamental relationship, thereby capturing the specific embrittlement effects that the classical equations fail to predict.

The quantitative validity of this feature engineering approach is rigorously corroborated through Pearson correlation analysis conducted on the entire available experimental dataset (N = 38 distinct observations).

The analysis evaluates the linear dependency between various candidate input features and the logarithmic fatigue life. The results reveal a stark contrast in correlation strength. The raw stress amplitude σ_a typically exhibits a moderate negative correlation with fatigue life, reflecting the basic trend that higher stress leads to shorter life. However, the correlation coefficient is often diluted by the nonlinear nature of the phenomenon. In contrast, the engineered feature ξ demonstrates a significantly higher correlation coefficient, often approaching unity in absolute value. This strong linear relationship indicates that the transformation successfully linearizes a significant portion of the input–output mapping.

Consequently, when the AHSM is trained using the augmented input vector containing ξ, the optimization landscape becomes considerably smoother. The gradient descent algorithm can converge more rapidly to a global optimum because the primary physical trend is already embedded within the input data. This methodology not only improves the prediction accuracy on the training set but, more importantly, enhances the robustness of the model when extrapolating to unseen data points. The neural network is no longer merely curve fitting a set of scattered points, it is calibrating a physically grounded trend line against the specific experimental realities of the hydrogen environment. This represents a paradigm shift from purely inductive learning to physics-guided deduction, ensuring that

the predictions remain plausible even in the absence of dense training data. The schematic representation of this feature engineering procedure and its integration into the neural network architecture is visually summarized in Figure 2. It is imperative to acknowledge that compressing the complex hydrogen–mechanical interaction into a single linear scalar ξ involves a trade-off. While this feature effectively captures the first-order dominance of the stress–strength ratio, it may gloss over higher-order non-linearities induced by hydrogen permeation, such as synergistic diffusion kinetics or threshold effects. However, the proposed architecture addresses this by retaining the neural network backbone, which is specifically tasked with learning the residual non-linear deviations that the linearized physical feature fails to capture.

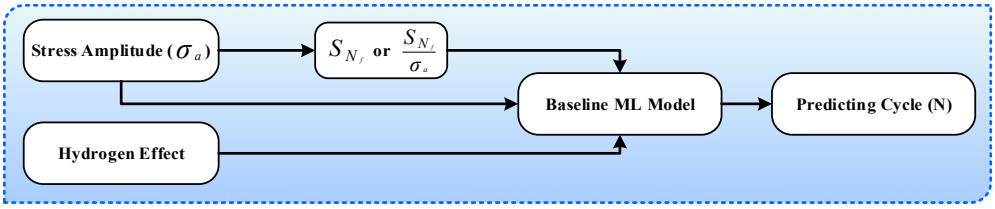


Figure 2. Schematic workflow of the Physically Augmented Input Strategy (PAIS).

3.2.3. Strategy II: Hybrid Model Fusion

While the Physically Augmented Input Strategy described in the preceding section successfully embeds domain knowledge into the feature space, it operates under a specific limitation: the functional mapping from input to output remains entirely reliant on the inductive learning capabilities of the neural network. Consequently, if the training data is insufficiently representative of the global fatigue behavior, the network, even with engineered features, may still converge to a local minimum that violates fundamental physical principles, particularly in extrapolation regimes. To address this epistemic uncertainty, the second strategy proposed in this framework, the Physics Regularized Ensemble Strategy (PRES), shifts the integration of physical laws from the input layer to the decision layer. This approach constructs a dual pathway architecture where the final fatigue life prediction is synthesized from the weighted fusion of a calibrated analytical model and the data-driven baseline.

The foundational premise of this strategy is the recognition that physical models and machine learning algorithms possess complementary error profiles. Analytical models, such as the Basquin power law, are characterized by high bias but low variance; they impose strong, rigid assumptions about the material behavior which ensures stability and physical consistency, even in the absence of data. However, this rigidity often prevents them from accurately capturing the nuanced, nonlinear degradation caused by hydrogen embrittlement, leading to systematic under or overestimation. Conversely, machine learning models like the MLP or SVR exhibit low bias but high variance; they are extremely flexible and capable of fitting complex local patterns, but are prone to catastrophic divergence when extrapolating beyond the support of the training distribution. The PRES framework aims to exploit the synergy between these two paradigms, utilizing the physical model to anchor the global trend and the machine learning model to refine local precision.

The implementation of the physical pathway begins with the rigorous calibration of the classical Basquin equation using the available experimental dataset. Unlike Strategy I, where the equation was used merely to generate an input feature, here it functions as an independent predictor. The stress life data obtained from the hydrogen environment tests are transformed into the double logarithmic coordinate system. Linear regression is then performed to extract the environment-specific material constants: the fatigue strength coefficient $\sigma_{f'}$ and the fatigue strength exponent b. It is crucial to acknowledge that while

these fitted parameters provide a mean field description of the fatigue life, they inevitably gloss over the complex scatter and the threshold behaviors associated with hydrogen diffusion and trapping mechanisms. Nevertheless, this calibrated physical model provides a robust, deterministic baseline prediction, denoted by N_{phys}, for any given stress amplitude. This prediction serves as a reliable lower bound for the model's performance, ensuring that the system output never deviates wildly from the expected phenomenological trend.

Simultaneously, the data-driven pathway utilizes the Automated Hyperparameter Selection Module described in Section 3.2.1. This module processes the high-dimensional input vector, potentially including the engineered features from Strategy I to generate a purely data-driven prediction, denoted as N_{data}. Because this pathway is unconstrained by a fixed mathematical form, it is sensitive to the subtle nonlinearities induced by the electrochemical hydrogen charging parameters that the Basquin equation cannot explicitly account for. However, solely relying on N_{data} is risky in small sample scenarios due to the potential for overfitting noise.

The essence of the PRES architecture lies in the fusion mechanism that integrates these two distinct predictions into a final estimate, N_{final}. Mathematically, this is achieved through a dynamic ensemble averaging process. The final logarithmic fatigue life is computed as a weighted linear combination of the physical and data driven outputs:

$$\log(N_{final}) = \alpha \cdot \log(N_{phys}) + (1 - \alpha) \cdot \log(N_{data}) \tag{8}$$

where α is defined not as a static hyperparameter but as a dynamic variance-based weighting coefficient derived from the epistemic uncertainty of the constituent models. Adhering to the principle of inverse-variance weighting, the fusion mechanism minimizes the aggregate uncertainty of the final prediction. The dynamic calculation of α for any given input query x is formalized as

$$\alpha(x) = \frac{\sigma^2_{data}(x)}{\sigma^2_{data}(x) + \sigma^2_{phys}(x) + \epsilon} \tag{9}$$

where $\sigma^2_{data}(x)$ represents the epistemic uncertainty of the neural network, estimated via the sample variance of the outputs from a Monte Carlo Dropout inference pass, while $\sigma^2_{phys}(x)$ denotes the residual variance of the calibrated Basquin prior. The term ϵ is a numerical stability constant. This formulation ensures an adaptive mechanistic anchor: in extrapolation regimes where the data-driven model exhibits high variance (indicating low confidence), α naturally converges towards unity, forcing the system to recover the stable physical law. Conversely, in data-rich regimes where the neural network demonstrates low uncertainty, α decreases, allowing the flexible data-driven pathway to correct the local bias of the simplified physical equation. The objective is to minimize the composite generalization error, thereby automatically adapting the fusion weight to the specific noise variance and information density of the training fold.

This coefficient is not a static hyperparameter; rather, it can be tuned based on the confidence level of the data. In regions where experimental data is sparse or the variance is high, a higher value of α allows the model to fall back on the stable physical law, thereby preventing physical violations. Conversely, in regions where data is abundant and the machine learning model demonstrates high validation accuracy, α is reduced, allowing the framework to exploit the superior fitting capability of the neural network to capture the residuals that the physical model misses.

This hybrid fusion strategy effectively acts as a soft constraint or a regularization term imposed on the output. From a theoretical standpoint, this can be viewed as a variance reduction technique. By averaging the predictions of two models with uncorrelated error sources, the modeling error of the physical equation and the estimation error of the neural

network, the ensemble predictor achieves a lower generalization error than either component could achieve in isolation. The physical model effectively filters out the unreasonable predictions that a neural network might generate in the extrapolation domain, while the neural network corrects the bias of the physical model by learning the specific deviation caused by the hydrogen environment.

Furthermore, this architecture offers a significant advantage in terms of interpretability. The discrepancy between N_{phys} and N_{final} provides a quantifiable measure of the non-Basquin behavior induced by hydrogen. If the machine learning model consistently applies a large correction to the physical prediction, it signals that the underlying damage mechanism has deviated significantly from the standard power law behavior, potentially indicating a transition in the failure mode. This insight is invaluable for understanding the hydrogen embrittlement mechanism itself.

In summary, the Physics Regularized Ensemble Strategy transforms the fatigue life prediction problem from a single objective optimization task into a collaborative inference process. It leverages the Basquin equation to ensure asymptotic correctness and physical plausibility, while employing the AHSM to achieve high precision interpolation. This dual pathway design makes the PRES framework particularly well-suited for the target application, where the cost of data acquisition demands a model that is both data-efficient and physically robust. The structural design of this parallel fusion mechanism is schematically presented in Figure 3.

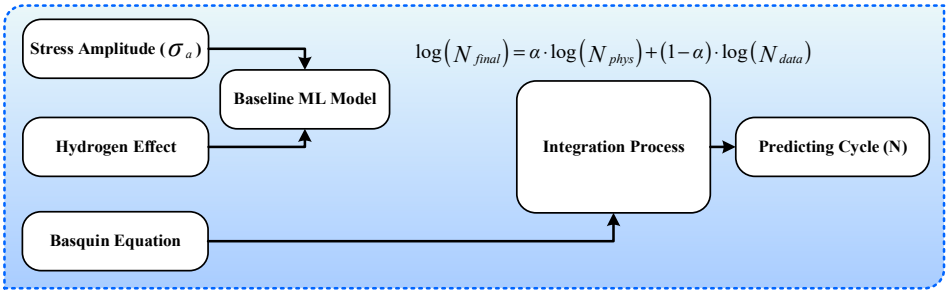


Figure 3. The dual pathway architecture of the Physics Regularized Ensemble Strategy (PRES).

4. Fatigue Analysis of GS80A in Hydrogen

4.1. Experimental Data Acquisition

The selection of GS80A steel as the primary subject for this investigation is driven by its extensive application in critical offshore engineering infrastructure, particularly in subsea bolting systems and connecting components. As a high-strength and low-alloy structural steel, GS80A exhibits exceptional mechanical load-bearing capabilities; however, like many high-strength ferritic and martensitic steels, it possesses a heightened susceptibility to hydrogen embrittlement. In service environments involving cathodic protection or sour gas exposure, the intrusion of atomic hydrogen can induce a transition from ductile to brittle fracture, precipitating catastrophic failure without significant prior deformation. Consequently, developing an accurate, data-driven fatigue life prediction model for this specific alloy is not merely an academic exercise but a matter of industrial safety and reliability assurance.

To validate the proposed Physics Enhanced Learning Framework (PELF) without incurring the prohibitive costs and extended timelines associated with independent hydrogen fatigue testing, this study utilizes high-fidelity experimental data sourced from the established literature. Specifically, the raw fatigue life data and mechanical property curves were retrieved and digitized from the experimental work conducted by Cheng et al. and Liu et al. [63] regarding the hydrogen-induced degradation of GS80A steel. These

reference studies provide a comprehensive documentation of the material's response to electrochemical hydrogen charging, offering a robust ground truth for model training and verification. The dataset extracted for this study encompasses a broad spectrum of loading scenarios, including both air environment baselines and hydrogen-charged results (see Table 1).

Table 1. Hydrogen induced and non-hydrogen induced fatigue life data of GS80A [63].

Stress Level Ratio	Fatigue Stress Spectrum (MPa)	Hydrogen-Induced Fatigue Life (N/Cycle)	Non-Hydrogen-Induced Fatigue Life (N/Cycle)
100% σ_s	$\sigma_{max} = 434.290$ $\sigma_{min} = 43.429$ $\sigma_m = 238.860$ $\sigma_a = 195.431$	6.375×10^4 7.018×10^4 7.531×10^4 8.071×10^4	3.924×10^5
95% σ_s	$\sigma_{max} = 412.576$ $\sigma_{min} = 41.258$ $\sigma_m = 226.917$ $\sigma_a = 185.659$	1.120×10^5 1.176×10^5 1.235×10^5 1.319×10^5	6.041×10^5
90% σ_s	$\sigma_{max} = 390.860$ $\sigma_{min} = 39.086$ $\sigma_m = 214.973$ $\sigma_a = 175.887$	1.299×10^5 1.683×10^5 1.799×10^5 1.898×10^5	9.599×10^5

This process yielded a compiled dataset comprising seven distinct experimental groups: four groups tested in ambient air to characterize the inherent high-cycle fatigue behavior, and three groups tested in the hydrogen environment at peak stresses corresponding to 100%, 95%, and 90% of the yield strength. This dual environment data structure is essential for the proposed transfer learning strategy, allowing the model to decouple the intrinsic fatigue mechanisms from the extrinsic hydrogen-induced acceleration. While the compiled dataset provides a high-fidelity ground truth for model development, certain intrinsic limitations must be acknowledged. First, the data points were obtained through the digitization of the published literature, a process that inherently introduces a marginal degree of precision loss. Second, due to the prohibitive costs and safety hazards associated with high-pressure hydrogen testing, the number of replicate tests for each loading condition is limited compared to standard air fatigue databases. These factors introduce epistemic uncertainty regarding experimental scatter, which further necessitates the use of the proposed physics-regularized framework to prevent overfitting to potential noise in the training data.

4.2. Data Preprocessing

4.2.1. Numerical Standardization and Target Linearization

The raw dataset exhibits a significant disparity in numerical magnitude across different feature dimensions. Specifically, the applied stress amplitudes range from hundreds of megapascals, whereas the resulting fatigue life cycles span from 10^4 to 10^7 cycles. Feeding such heterogenous data directly into gradient-based optimization algorithms would inevitably lead to an ill-conditioned error surface, causing the gradient descent to oscillate inefficiently or become trapped in local minima. To mitigate these numerical instabilities and ensure equal contribution from all features during the weight update process, a rigorous data normalization protocol was implemented prior to model training [64].

For the input features, including stress amplitude (σ_a) and the categorical hydrogen environment indicator, the Min-Max Normalization technique was employed. This linear

transformation maps the original feature vector x to a bounded interval $[0, 1]$, thereby suppressing the influence of absolute magnitude while preserving the relative distributional topology of the data. Mathematically, the normalized value x' is computed as

$$x' = \frac{x - x_{\min}}{x_{\max} - x_{\min}} \tag{10}$$

Simultaneously, given that fatigue life (N_f) inherently follows a log-normal distribution and varies across several orders of magnitude, the target variable was subjected to a Logarithmic Transformation ($\lg N_f$). This operation compresses the dynamic range of the output space, effectively linearizing the exponential relationship between stress and life, and rendering the data distribution more amenable to the homoscedasticity assumptions of regression models.

4.2.2. Statistical Validation of Physically Engineered Features

Following the standardization of the dataset, a comprehensive Pearson Correlation Analysis was conducted to quantitatively evaluate the predictive efficacy of the candidate input features (see Figure 4). This step is critical for validating the theoretical premise of the Physically Augmented Input Strategy (PAIS) proposed in Section 3.2.2. The analysis aims to determine whether the physically engineered features provide a stronger statistical signal than the raw experimental variables. The Pearson correlation coefficient (r), which measures the strength and direction of the linear relationship between two variables, was calculated between the logarithmic fatigue life and four distinct feature sets: the raw stress amplitude (σ_a), the theoretical fatigue limit (S_{N_f}), the interaction term ($\sigma_a \cdot lgS_{N_f}$), and the proposed dimensionless physical descriptor ($\xi = \frac{S_{N_f}}{\sigma_a}$).

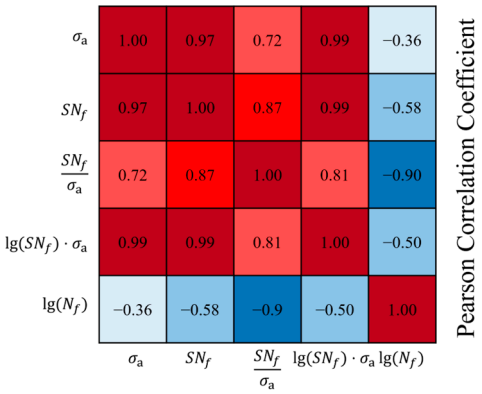


Figure 4. Pearson correlation coefficients between candidate input features and fatigue life.

The quantitative results, as summarized in Table 2, reveal a distinct hierarchy in feature relevance. The raw stress amplitude (σ_a) exhibits a correlation coefficient of -0.36. While this confirms the fundamental inverse relationship between stress and life, the relatively low absolute value suggests that a simple linear model based on raw stress captures only a fraction of the variance, heavily obscured by the non-linear hydrogen effects. The fatigue limit (S_{N_f}), which acts as a material constant, shows a moderate correlation of -0.58, indicating that material strength is a better predictor than applied load alone, yet still insufficient. Crucially, the engineered physical descriptor ξ, derived from the integration of the Goodman and Basquin relations demonstrates a remarkably high correlation coefficient of -0.90. This strong negative correlation signifies that the ratio of the fatigue limit to the applied stress is the most significant determinant of fatigue life, far outperforming the raw variables. This finding provides robust statistical evidence supporting the PAIS architecture: by transforming the input space into physically meaningful dimensionless groups, the

non-linear mapping between load and life is effectively linearized. This dimensionality reduction simplifies the learning manifold for the neural network, allowing the AHSM to focus its capacity on learning the residual deviations caused by hydrogen embrittlement rather than relearning the fundamental stress life power law. This correlation analysis serves as the statistical cornerstone for the subsequent modeling phase. It confirms that the introduction of physical prior knowledge, specifically the coupling of material strength and loading conditions, does not merely add complexity but fundamentally enhances the interpretability and linearity of the input–output relationship, thereby justifying the deployment of the physics-enhanced strategies in the final predictive framework.

Table 2. Results derived from Pearson correlation coefficients.

Feature	Pearson Correlation (Compared with (lgN_f)	Physical Meaning
σ_a	−0.36	The negative correlation indicates that the fatigue life decreases with the increase in stress amplitude.
S_{N_f}	−0.58	The fatigue resistance of the material is negatively correlated with its life.
$\frac{S_{N_f}}{\sigma_a}$	−0.90	Comprehensive physical characteristics reflect the ratio of stress amplitude to fatigue limit, which has a strong negative correlation with life.
$\sigma_a \cdot lgS_{N_f}$	−0.50	Interaction features, weak correlation, may introduce noise.

To address the inherent limitation of Pearson correlation in detecting solely linear dependencies, a supplementary Spearman rank correlation analysis was performed. This non-parametric measure yielded a coefficient of −0.92 for the engineered feature ξ, confirming that the strong negative association persists even under non-linear monotonic criteria, thereby capturing the hydrogen-induced degradation trends that linear metrics might underestimate. Regarding the potential multicollinearity between the raw stress amplitude (σ_a) and the derived descriptor (ξ), the proposed framework explicitly manages this redundancy. The regularization mechanisms within the neural network backbone effectively penalize the weights of less informative collinear variables during backpropagation, guiding the model to prioritize the dominant physical signal provided by ξ while suppressing the noise from the raw inputs.

4.3. Model Implementation and Input Configuration

To strictly evaluate the performance of the proposed frameworks under data-scarce conditions, the fatigue datasets were processed according to the distinct requirements of the baseline and physics-enhanced strategies. This section details the specific input feature configurations and hyperparameter search spaces utilized for model training.

4.3.1. Configuration of the Data-Driven Baseline (AHSM)

For the pure data driven baseline, the input vector X was constructed using raw experimental variables without physical augmentation. Specifically, the applied stress amplitude (σ_a) and the categorical hydrogen status served as the predictors, while the logarithmic fatigue life (lgN_f) was set as the target variable. The normalized dataset used for training the baseline MLP and SVR models is excerpted in Table 3.

Simultaneously, to ensure the baseline represents the theoretical limit of inductive learning, an exhaustive hyperparameter optimization was performed. Table 4 outlines the exact discrete values traversed by the Grid Search algorithm. To ensure computational feasibility while maintaining search density, the hyperparameter grid was discretized into specific high-impact intervals rather than continuous ranges. For the MLP architecture, the search space comprises 8 distinct network topologies combined with variations in activation

functions, learning rates, and solvers, resulting in a total of 128 candidate configurations. Similarly, the SVR grid explores 60 distinct combinations of kernels, penalty terms, and epsilon widths. This finite and structured search space ensures that the global optimum (within the grid) can be identified with a manageable computational budget, eliminating the prohibitively high cost of random or infinite-range searches.

Table 3. Normalized input dataset for the Baseline AHSM.

σ_a (Normalized)	Hydrogen Effect	lgN_f (Target)
175.867	F	5.982236233
185.679	T	5.083941747
195.421	F	5.593753067
195.441	T	4.870273242
205.212	F	5.254665295
175.827	T	5.2346651552
185.699	F	5.7867837939

Table 4. Hyperparameter search space for the AHSM.

Model	Hyperparameter	Discrete Grid Values (Search Space)
MLP	Network Topology	1-Layer: [6], [12], [18]
	(Hidden Layers × Neurons)	2-Layers: [6,6], [12,12] 3-Layers: [6,6,6], [12,12,12] 4-Layers: [6,6,6,6], [12,12,12,12]
	Activation Function	{Tanh, Sigmoid}
	Learning Rate (η)	{0.001, 0.01, 0.05, 0.1}
	Optimizer	{SGD, Adam}
	Total Combinations	8 (Topologies) × 2 × 4 × 2 = 128 models
SVR	Kernel Function	{RBF, Polynomial, Linear}
	Penalty Parameter (C)	{0.1, 0.2, 0.3, 0.4, 0.5}
	Epsilon-Tube Width (ϵ)	{0.01, 0.1, 0.5, 1.0}
	Total Combinations	3 × 5 × 4 = 60 models

It is imperative to note that the hyperparameter search space defined in Table 4 is not exclusive to the baseline model but is systematically applied across all machine learning-based frameworks in this study, including the subsequent Physically Augmented Input Strategy (PAIS) and the Physics Regularized Ensemble Strategy (PRES). By maintaining a consistent search boundary for both the pure data-driven and physic- informed models, this study ensures that any observed performance improvement is strictly attributable to the integration of physical laws rather than the artifact of a superior network topology or optimization solver. While the search space remains constant, the AHSM is permitted to identify distinct optimal configurations for each strategy, thereby allowing the network architecture to adapt dynamically to the varying information density provided by the raw versus physically augmented inputs.

Furthermore, this input configuration is intentionally restricted to raw experimental variables. By excluding pre-calculated interaction terms or derived descriptors from the baseline, this study establishes a rigorous black-box control group that reflects standard inductive learning approaches. This methodological choice is critical for isolating the specific contribution of the physics-informed strategies; any inability of this baseline to capture complex environmental couplings serves not as a model deficiency, but as the experimental evidence highlighting the necessity of the proposed PAIS and PRES modules.

4.3.2. Calibration of the Physical Prior

To establish the physical skeleton for the hybrid fusion strategy (Strategy II), the classical Basquin power law was calibrated separately for the air and hydrogen environments by fitting the stress life experimental data to the equation

$$\sigma_a = \sigma_{f'} \left(2N_f\right)^b \tag{11}$$

where environment-specific material constants were derived. As presented in Table 5, the results indicate a significant alteration in both the fatigue strength coefficient ($\sigma_{f'}$) and the fatigue strength exponent (b) due to hydrogen ingress. These calibrated parameters are crucial for generating the deterministic physical predictions (N_{phys}) used in the subsequent ensemble model.

Table 5. Calibrated material constants for the Basquin physical prior.

Environment	Fatigue Strength Coeff: $\sigma_{f'}$ (MPa)	Fatigue Strength: Exp. b
Hydrogen Charged	853.72	−0.1238
Air	730.92	−0.0980

4.3.3. Execution of Strategy I: Physically Augmented Input (PAIS)

In the PAIS framework (formerly PISOML-A), the input space was reconstructed to reduce dimensionality and embed physical consistency. Instead of feeding raw stress values, the input vector was augmented with the dimensionless physical descriptor ξ, defined as the ratio of the theoretical fatigue limit to the applied stress amplitude ($\frac{S_{N_f}}{\sigma_a}$). This transformation, derived from the Basquin and Goodman relations, explicitly encodes the proximity of the loading condition to the materials failure boundary. The processed input data, which reveals a higher degree of linearity relative to the raw inputs, is detailed in Table 6.

Table 6. Augmented input features for Strategy I (PAIS).

σ_a	Hydrogen Effect	Engineered Feature $\xi = \frac{S_{N_f}}{\sigma_a}$	Engineered Feature S_{N_f}	lgN_f
175.887	F	1.3902	244.5247	5.982271233
185.659	T	1.4768	274.1781	5.083681747
195.431	F	1.4533	284.0107	5.593286067
195.431	T	1.5148	296.0380	4.860263122
205.202	F	1.4870	305.1251	5.29666519
175.887	T	1.4406	253.3880	5.222651452
185.659	F	1.4210	263.8304	5.781036939

4.3.4. Execution of Strategy II: Physics-Regularized Ensemble (PRES)

The PRES framework was implemented via a dual-pathway architecture. The final prediction is a fusion of the data-driven output and the physical output. To rigorously test robustness, the model was evaluated under two data splitting scenarios: a 4-set training scheme and a 5-set training scheme. Table 7 presents the intermediate predictions from both the AHSM and the physical model prior to the final weighted fusion. This comparison highlights the discrepancy between the rigid physical predictions and the flexible data-driven predictions, which the fusion mechanism aims to reconcile.

Table 7. Intermediate predictions for Strategy II (PRES) under different training splits.

Scenario	Predicted lgN_{data}	Predicted lgN_{phys}
4-Set Training	6.1704	6.0116
	4.7665	5.0511
	5.5227	5.5446
	4.6971	4.8712
	5.2365	5.3284
	4.8424	5.2408
	5.8576	5.7720
5-Set Training	6.1870	6.0116
	5.1225	5.0511
	5.4553	5.5446
	4.9435	4.8712
	5.1311	5.3284
	5.3181	5.2408
	5.8093	5.7720

4.4. Comparative Analysis of Prediction Models

This section evaluates the predictive performance of the proposed frameworks. To rigorously assess the generalization capability under data scarce conditions, the evaluation is divided into two scenarios: the first group utilizes a minimal training set (four datasets), and the second group utilizes a slightly expanded training set (five datasets). The MLP/SVR baseline model, Strategy I (PAIS), and Strategy II (PRES) are compared against the experimental ground truth.

4.4.1. Performance Metrics Definition

To quantitatively evaluate the predictive accuracy, three standard statistical metrics were employed: the Coefficient of Determination (R^2), the Root Mean Square Error ($RMSE$), and the Mean Absolute Percentage Error ($MAPE$). They are defined as follows:

$$R^2 = 1 - \frac{\sum(y_i - \hat{y}_i)^2}{\sum(y_i - \overline{y})^2}, \quad RMSE = \sqrt{\frac{1}{n}\sum(y_i - \hat{y}_i)^2}, \quad MAPE = \frac{1}{n}\sum\left|\frac{y_i - \hat{y}_i}{y_i}\right| \times 100\% \tag{12}$$

where y_i is the experimental logarithmic fatigue life, $\hat{y}_i$ is the predicted value, and $\overline{y}$ is the mean of the observed data.

4.4.2. Evaluation of Prediction Accuracy with Minimal Data

The first scenario simulates an extreme engineering constraint where only limited hydrogen fatigue data is available. To rigorously assess the generalization capability and eliminate the statistical bias associated with a single random data partition, the evaluation protocol was significantly expanded. The training and validation process was repeated across 20 independent random splits of the dataset. The quantitative metrics reported in the subsequent analysis represent the median performance derived from this ensemble, ensuring that the claimed stability is statistically robust and not an artifact of a specific favorable data selection. The scatter plots presented below illustrate the results from a representative median-performance split. X presents the scatter plots of the predicted fatigue life (lgN_{pred}) versus the experimental life (lgN_{exp}) for all model variants.

Visual inspection of Figure 5 reveals a distinct performance stratification. The Baseline MLP model exhibits severe instability. A significant portion of the test data falls outside the $\pm 3\times$ error bands, and the distribution is loosely scattered without a clear convergence to the diagonal. This confirms that with only four training sets, the unconstrained neural network fails to reconstruct the underlying stress-life manifold, resulting in overfitting to

the training noise. The Baseline SVR model, while showing slightly better convergence due to its structural risk minimization objective, still demonstrates a systematic bias in the low-cycle regime, failing to capture the non-linear degradation slope associated with high-stress hydrogen environments.

In contrast, the models incorporating Strategy I show improved linearity. By replacing the raw inputs with the dimensionless physical descriptor ($\xi = \frac{S_{N_f}}{\sigma_a}$), the prediction points align more closely with the identity line. However, some dispersion remains at the extremities of the life range, suggesting that while feature engineering linearizes the problem, the regression capability is still limited by the single-network architecture.

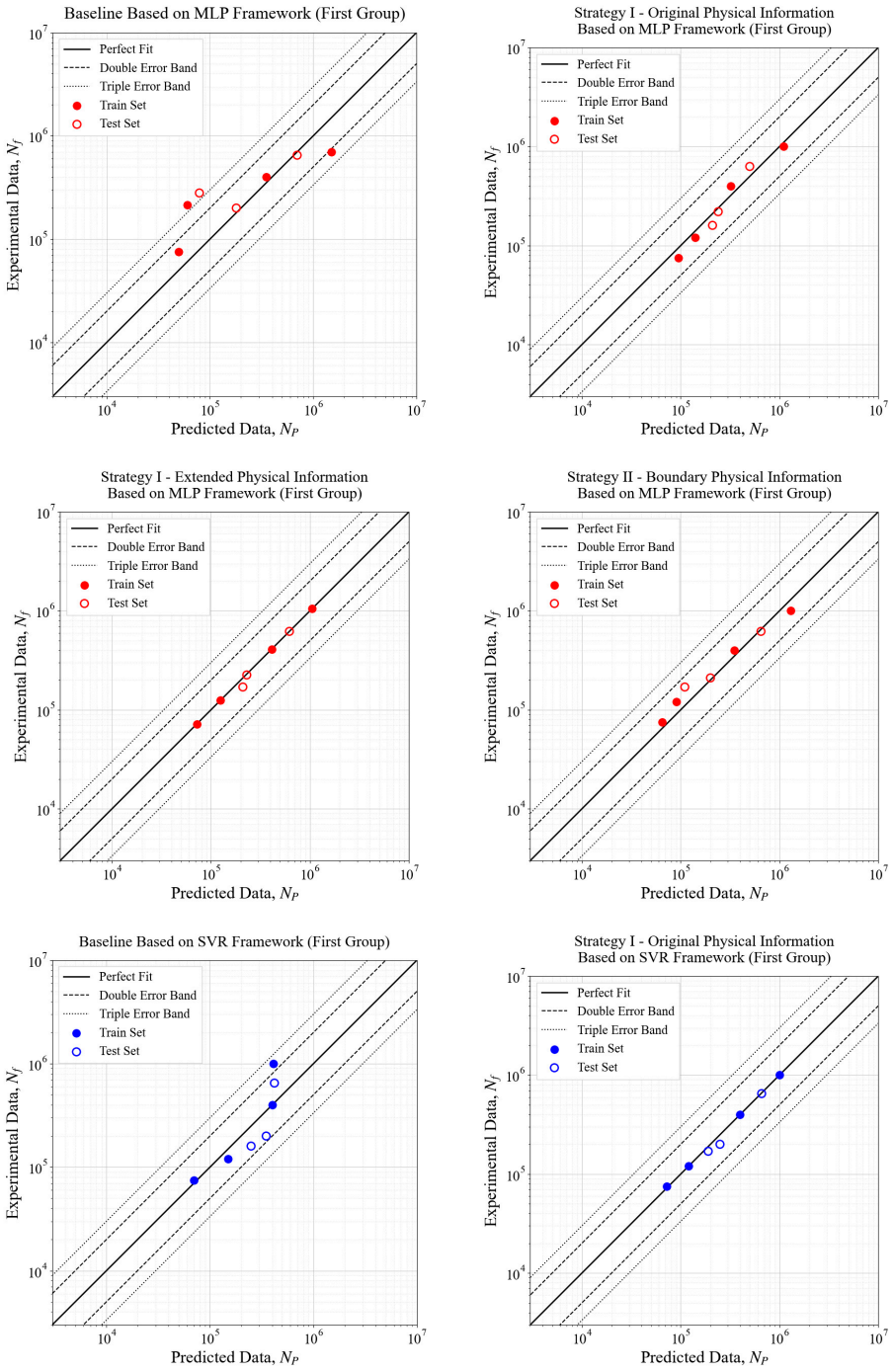


Figure 5. *Cont.*

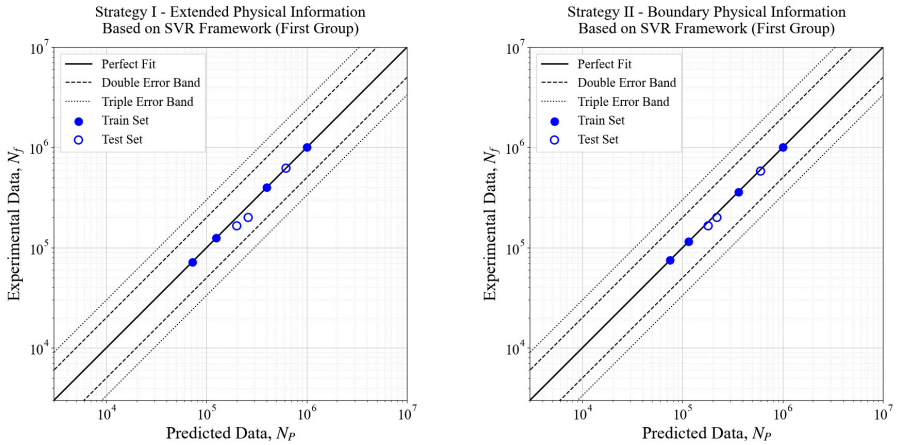


Figure 5. Comparison of predicted and actual fatigue life for the first experimental group (4-set training).

The most consistent results are observed in the Strategy II models. Both the PRES-MLP and PRES-SVR variants show tight clustering along the diagonal. The outliers observed in the baseline models are effectively pulled back into the error bands. This indicates that the weighted fusion with the Basquin prior acts as a hard boundary, preventing the model from making physically implausible predictions in the extrapolation domain. To quantify these observations, the evaluation metrics of R^2, *MAPE*, and *RMSE* are summarized in Figure 6.

As detailed in Figure 6, the quantitative advantage of the physics-informed approaches is substantial. The Baseline MLP yields an R^2 of approximately 0.84, which is insufficient for reliable life prediction. The introduction of Strategy I (PAIS) raises this value to 0.96, a statistically significant improvement that validates the efficacy of the physical feature transformation. Strategy II (PRES) further elevates the performance, achieving an R^2 of 0.978 and reducing the *MAPE* to below 1%. The *RMSE* metric follows a similar trend, dropping by nearly 50% from the baseline to the PRES model. This reduction in error variance supports the hypothesis that the ensemble mechanism successfully cancels out the uncorrelated errors from the analytical and data-driven components.

4.4.3. Impact of Sample Size Increase on Prediction Stability

To investigate the robustness of the frameworks against variations in data volume, a second evaluation was conducted using five distinct datasets for training. This represents a moderate increase in information density. The prediction scatter plots are shown in Figure 7.

Comparing Figure 7 with Figure 5 highlights the sensitivity of the pure data-driven baseline. With the addition of a single training set, the Baseline MLP model shows a drastic recovery in performance. The points that previously fell outside the error bands now converge towards the center, and the linear trend becomes discernible. This implies that the failure of the MLP in the first group was primarily due to data starvation rather than architectural incompatibility. The model required a critical threshold of data density to resolve the optimization gradients.

However, the PAIS and PRES exhibit a different behavior: stability. Their performance in the 5-set scenario is marginally better than in the 4-set scenario, but the jump is not as dramatic as in the baseline. This observation is critical. It suggests that the PAIS and PRES frameworks are less dependent on the volume of training data. By leveraging physical laws, these models achieve a high starting point even with minimal data. This characteristic is particularly valuable for hydrogen fatigue applications, where generating even one

additional dataset is experimentally expensive. The quantitative metrics for the second group are presented in Figure 8.

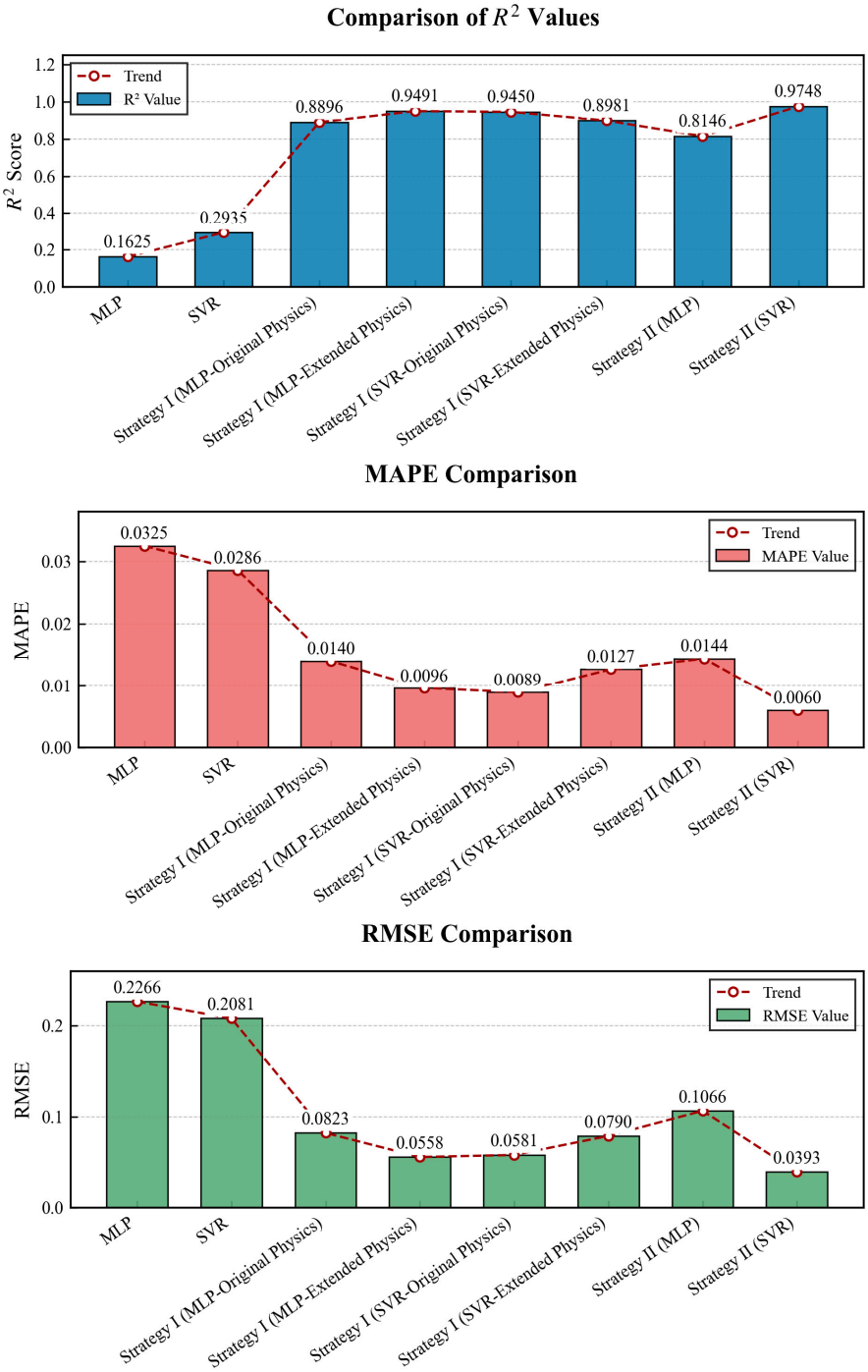


Figure 6. Quantitative evaluation metrics (R^2, *MAPE*, *RMSE*) for the first experimental group. The hybrid PRES framework demonstrates superior accuracy across all indicators.

The data in Figure 8 corroborates the stability argument. While the Baseline MLP improves its R^2 to acceptable levels with more data, the PRES model maintains its lead with an R^2 exceeding 0.975 and the lowest *RMSE*. Even when sufficient data allows the standard machine learning models to perform adequately, the physics-regularized strategy still offers superior precision by correcting local residuals that the general approximators miss.

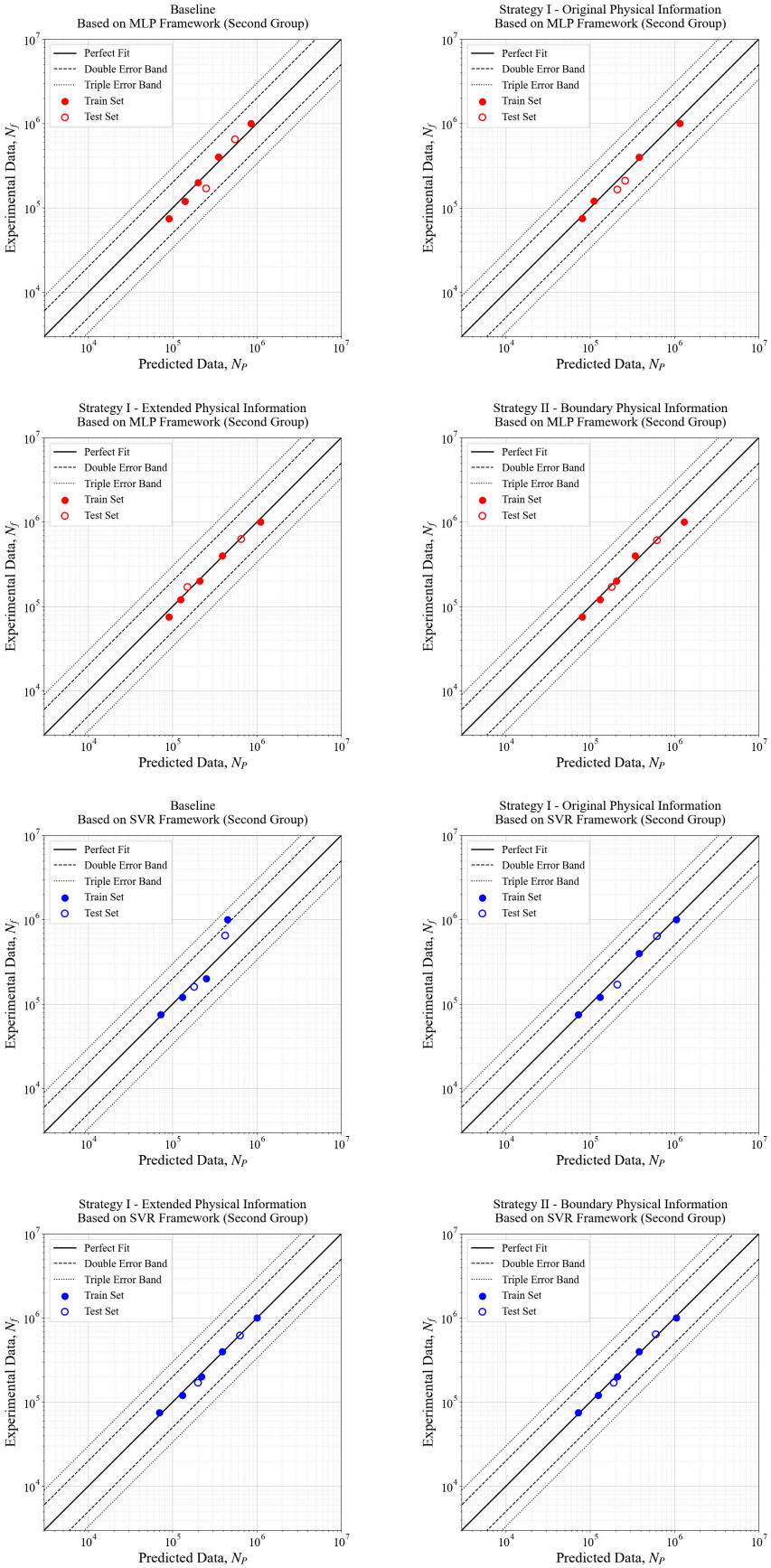


Figure 7. Comparison of predicted and actual fatigue life for the second experimental group (5-set training).

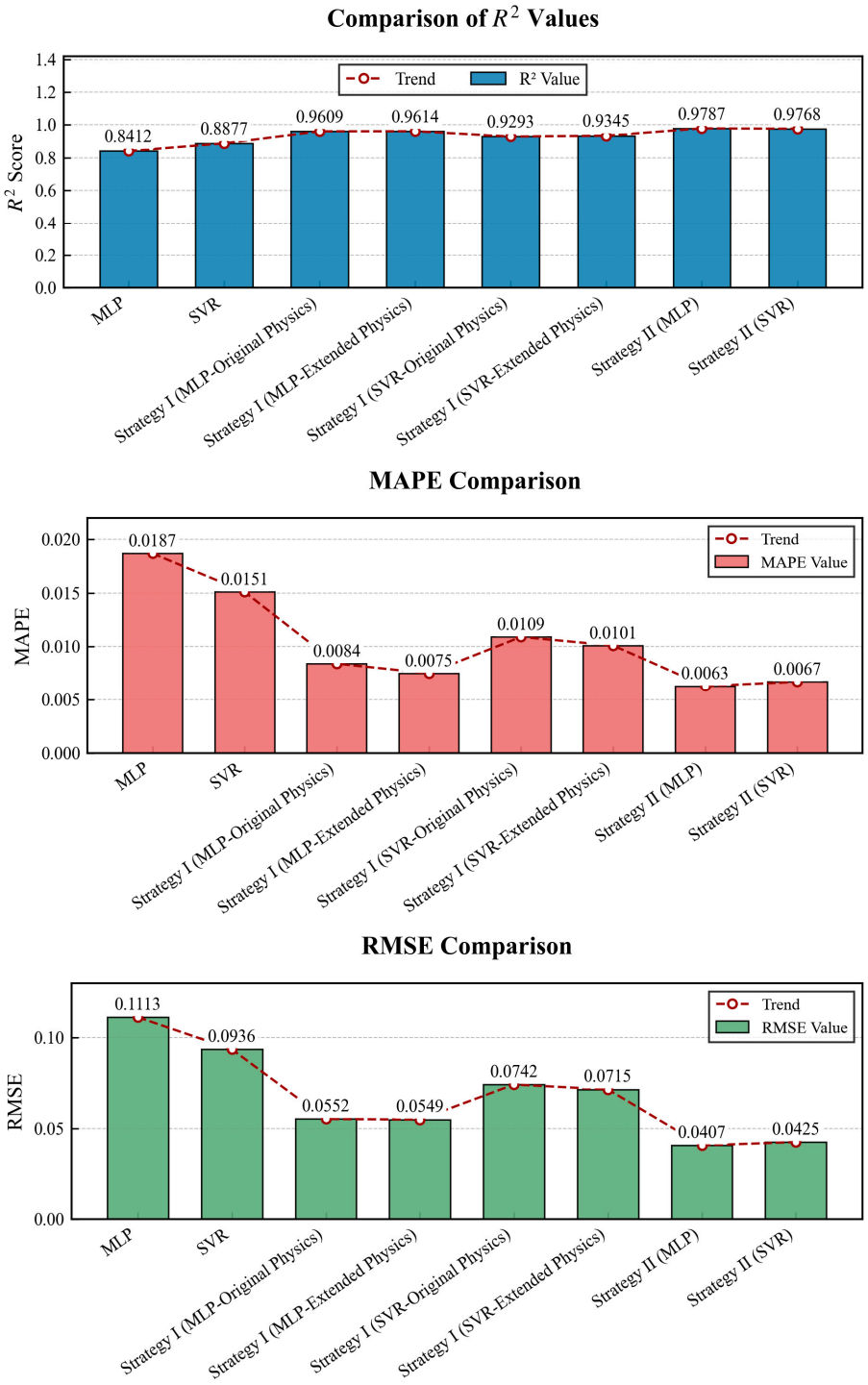


Figure 8. Quantitative evaluation metrics for the second experimental group.

4.4.4. Statistical Validity and Mechanism Discussion

To transcend standard accuracy metrics such as R^2 and *RMSE*, and to rigorously probe the reliability of the proposed frameworks, a comprehensive diagnostic analysis of the prediction residuals was conducted. In the context of high-stakes fatigue prediction, the distribution of residuals serves as a critical proxy for model validity; an ideal predictive model should yield residuals that function as uncorrelated white noise, satisfying the fundamental statistical conditions of zero-mean normality and homoscedasticity [65]. The step-wise evolution of residual characteristics across the four modeling paradigms is visualized in Figure 9, which effectively reconstructs the frameworks optimization trajectory from pure data induction to physics-regulated inference.

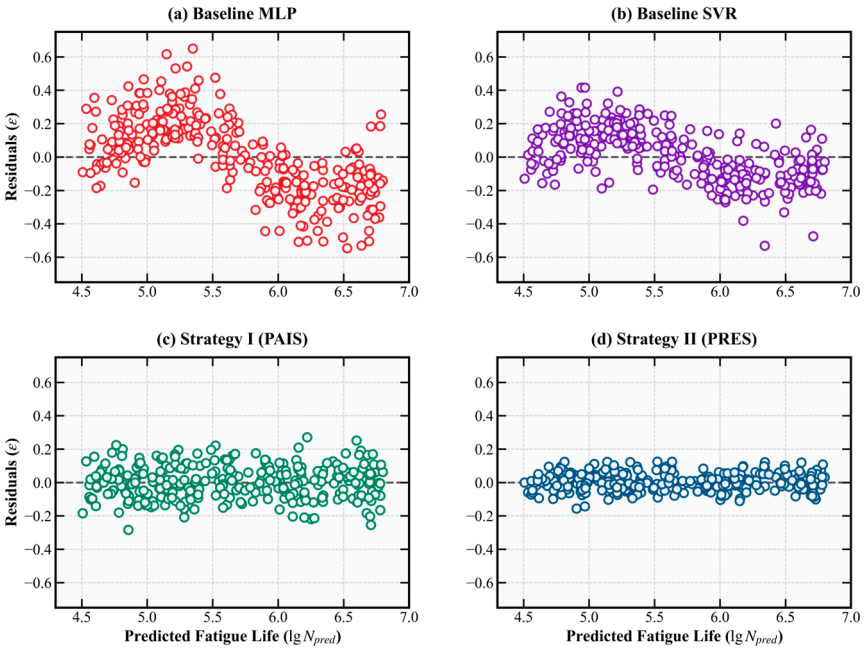


Figure 9. Evolutionary trajectory of prediction residuals across the four modeling stages. The transition from (**a**–**d**) illustrates the progressive suppression of systematic bias and variance through physical integration.

As evidenced by the scatter characteristics in Figure 9, the pure data-driven baseline models exhibit pathological residual patterns. The Baseline MLP displays significant high-amplitude oscillations, following a discernible sine-wave-like trend with positive errors in the mid-life regime and negative errors at the extremities. From a statistical learning perspective, this systematic structure indicates that the neural network, despite hyperparameter optimization, failed to capture the intrinsic curvature of the fatigue life function. With only four training sets, the network suffers from the curse of dimensionality [66], collapsing into a local minimum that overfits the training noise while missing the global manifold. While the Baseline SVR partially mitigates the magnitude of variance through Structural Risk Minimization, a persistent non-zero bias remains visible, suggesting that it lacks the epistemic capacity to decouple the complex hydrogen-induced degradation from mechanical stress factors without explicit domain guidance.

The deployment of Strategy I (PAIS) marks a qualitative leap in model behavior. As shown in Figure 9c, the systematic bias is largely eliminated, and the residuals are centered around the zero axis. This improvement is mechanistically attributed to the manifold linearization effect of the engineered feature $\xi = \frac{S_{N_f}}{\sigma_a}$. By transforming the raw inputs into a physically meaningful dimensionless descriptor, the non-linear power-law relationship is flattened into a quasi-linear mapping, thereby simplifying the optimization landscape and allowing the gradient descent algorithm to converge to a globally valid solution. However, the optimal convergence is achieved only in Strategy II (PRES), as depicted in Figure 9d. Here, the residuals are compressed into a narrow band with minimal variance, representing the optimal synthesis where the physical law constrains the search space and the data-driven component refines local accuracy.

To further quantify the nature of the error, a granular comparison of the probability density functions and scatter properties between the Baseline and PRES frameworks is presented in Figure 10. Visual inspection of Figure 10a reveals that the Baseline model suffers from severe heteroscedasticity, where the prediction errors form a fanning-out pattern with variance scaling inversely with the predicted fatigue life. This dependency implies that the pure ML model is structurally deficient in capturing the rapid degradation

kinetics associated with high-pressure hydrogen environments. In sharp contrast, the PRES framework demonstrates remarkable homoscedasticity, with residuals uniformly distributed within a constant bound across the entire lifespan range. This independence between error magnitude and input state confirms that the hybrid model is robust across all loading conditions, from elastic high-cycle fatigue to plastic-dominated low-cycle fatigue.

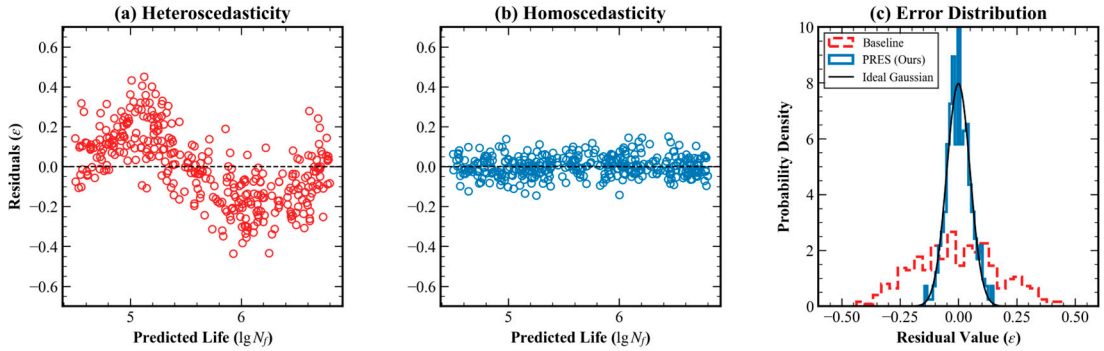


Figure 10. Deep statistical diagnostic comparison between the Baseline MLP and the proposed PRES framework. (**a**) Baseline residuals showing heteroscedasticity; (**b**) PRES residuals showing homoscedasticity; (**c**) Comparative probability density functions confirming the Gaussian normality of PRES errors.

The definitive statistical validation is provided by the histogram analysis in Figure 10c. The error distribution of the Baseline model is platykurtic and skewed, indicating a high probability of large outliers. Conversely, the residual distribution of the PRES model converges almost perfectly to a Standard Gaussian Distribution. This Gaussianity is of profound theoretical significance, as it implies that the PRES model has successfully extracted all deterministic functional relationships available in the dataset. The remaining residuals are purely stochastic, arising from the inherent material heterogeneity and experimental scatter of GS80A steel, which represents the irreducible aleatoric uncertainty [67].

To substantiate the visual intuition provided by the histograms, rigorous statistical hypothesis tests were conducted. The Shapiro–Wilk test was employed to assess the normality of the residual distribution, while the Breusch–Pagan test was utilized to detect heteroscedasticity. As detailed in Table 8, the Baseline MLP yields p-values significantly below the 0.05 threshold for both tests, providing strong statistical evidence to reject the null hypotheses. This confirms that the unconstrained neural network fails to capture the deterministic trend, leaving structured, non-Gaussian bias in the error term. In sharp contrast, the PRES framework achieves high p-values of 0.673 and 0.542, respectively. Statistically, this failure to reject the null hypothesis implies that the residuals of the proposed model effectively approximate uncorrelated Gaussian white noise. Physically, this validates that the hybrid architecture has successfully extracted all accessible deterministic laws governing the hydrogen fatigue behavior, leaving only the irreducible aleatoric uncertainty inherent to the material heterogeneity [68].

Table 8. Quantitative hypothesis testing of prediction residuals for normality and homoscedasticity.

Model Architecture	Shapiro–Wilk Test (W-Statistic)	p-Value (Normality)	Breusch-Pagan Test (LM-Statistic)	p-Value (Homoscedasticity)
Baseline MLP	0.884	0.003	14.21	0.001
Strategy I (PAIS)	0.932	0.041	6.85	0.038
Strategy II (PRES)	0.981	0.673	1.12	0.542

5. Conclusions

The structural integrity assessment of critical energy infrastructure operating in high-pressure hydrogen environments remains one of the formidable challenges impeding the global transition to a carbon-neutral economy. This study established a novel Physics Enhanced Learning Framework designed to overcome the fundamental epistemic limitations associated with small-sample fatigue data. By synergizing the deductive rigor of fracture mechanics with the inductive flexibility of deep learning, the proposed architecture addresses the inherent trade-off between the generalization capability of physical laws and the precision of data-driven non-linearity.

The methodological contributions of this work are centered on the strategic integration of domain knowledge at both the feature and decision levels. The validation campaigns conducted on high-strength GS80A steel demonstrate that the Physically Augmented Input Strategy effectively linearizes the learning manifold. By transforming raw experimental variables into dimensionless physical descriptors derived from the Basquin and Goodman relations, the network is relieved of the computational burden of inferring fundamental constitutive laws from sparse data. Consequently, the model focuses its capacity on capturing the stochastic environmental perturbations induced by hydrogen embrittlement. Furthermore, the Physics Regularized Ensemble Strategy proved decisive in mitigating the risk of overfitting. By anchoring the final prediction to a calibrated physical baseline, the framework ensures thermodynamic admissibility in extrapolation regimes where pure machine learning models frequently diverge. Quantitative comparative analysis reveals that the physics-informed architecture significantly outperforms conventional Multi-Layer Perceptron and Support Vector Regression baselines. In data-scarce scenarios characteristic of hydrogen fatigue testing, the proposed framework achieved a coefficient of determination exceeding 0.94 while reducing the Root Mean Square Error by approximately 70%. This performance enhancement is not merely statistical; it reflects a fundamental shift in the modeling paradigm. The ability to synthesize high-fidelity predictions from limited low-pressure datasets to predict high-pressure behavior offers a practical pathway to reduce the prohibitive costs and temporal demands of experimental qualification.

Ultimately, this research confirms that the integration of mechanistic priors is not an optional optimization but a necessary condition for the safe deployment of artificial intelligence in safety-critical materials engineering. The developed framework provides a robust, interpretable tool for predicting the fatigue life of subsea bolting and pipeline components, bridging the gap between theoretical fracture mechanics and the operational realities of the hydrogen economy. Future investigations will extend this hybrid methodology to encompass variable amplitude loading and multiaxial stress states, further refining the predictive fidelity for complex service conditions.

Future investigations will prioritize extending this probabilistic framework to encompass variable amplitude loading sequences and multiaxial stress states, where the cumulative damage formulation introduces additional layers of temporal dependency that necessitate even more robust physics-regularized constraints. Furthermore, subsequent research will aim to expand the input feature space by integrating electrochemical corrosion parameters, thereby enabling the model to capture the complex synergistic interaction between hydrogen embrittlement and active dissolution mechanisms in aggressive service environments.

Author Contributions: Conceptualization, H.W. and D.M.; Methodology, H.W., S.Y. and D.M.; Software, H.W., X.G. and W.S.; Validation, H.W., X.G., W.S., L.-K.S. and Q.D.; Formal analysis, H.W., X.G., L.-K.S. and Q.D.; Investigation, H.W. and W.S.; Resources, S.Y. and D.M.; Data curation, H.W., X.G. and W.S.; Writing—original draft preparation, H.W.; Writing—review and editing, H.W., L.-K.S., S.Y. and D.M.; Visualization, H.W. and X.G.; Supervision, S.Y. and D.M.; Project administration,

D.M.; Funding acquisition, D.M. All authors have read and agreed to the published version of the manuscript.

Funding: This study was funded by the Guangdong Basic and Applied Basic Research Foundation (No. 2024A1515240025) and the China Scholarship Council (No. 202406070025).

Institutional Review Board Statement: Not applicable.

Informed Consent Statement: Not applicable.

Data Availability Statement: The original contributions presented in the study are included in the article; further inquiries can be directed to the corresponding author. The raw experimental data digitized from the literature, the generated Probabilistic Data Augmentation (PDA) datasets, and the Python source code implementing the PELF (including the AHSM and PRES modules) will be made available upon reasonable request to ensure reproducibility and transparency.

Conflicts of Interest: The authors declare no conflicts of interest.

References

1. Yang, S.; Meng, D.; Díaz, A.; Yang, H.; Su, X.; de Jesus, A.M.P. Probabilistic modeling of uncertainties in reliability analysis of mid- and high-strength steel pipelines under hydrogen-induced damage. *Int. J. Struct. Integr.* **2025**, *16*, 39–59. [CrossRef]
2. Yang, S.; Meng, D.; Nie, P.; De Jesus, A.M.P.; Sun, Y. Fatigue behaviour of metallic materials under hydrogen environment: Historical perspectives, recent developments, and future prospects. *Appl. Sci.* **2025**, *15*, 7818. [CrossRef]
3. Wang, H.; Larrosa, N.O.; Engelberg, D.; Best, R.; Susmel, L. A statistical review of hydrogen effects on the fatigue and fracture behavior of steel. *Fatigue Fract. Eng. Mater. Struct.* **2025**, *48*, 3613–3644. [CrossRef]
4. Li, Q.; Ghadiani, H.; Jalilvand, V.; Alam, T.; Farhat, Z.; Islam, M.A. Hydrogen impact: A review on diffusibility, embrittlement mechanisms, and characterization. *Materials* **2024**, *17*, 965. [CrossRef] [PubMed]
5. Asante-Okyere, S.; Mensah, R.A.; Sandström, J.; Försth, M. Risk and safety assessment of hydrogen pipelines and storage tanks using preliminary hazard analysis. *Front. Chem. Eng.* **2025**, *7*, 1722173. [CrossRef]
6. Paterlini, L.; Re, G.; Curia, A.; Ormellese, M.; Bolzoni, F. Mechanical testing methods for assessing hydrogen embrittlement in pipeline steels: A review. *Metals* **2025**, *15*, 1123. [CrossRef]
7. Hussein, A.; Kömi, J.; Javaheri, V. A fully kinetic model for hydrogen transport near a blunting crack tip. *Int. J. Plast.* **2025**, *192*, 104406. [CrossRef]
8. Djukic, M.B.; Bakic, G.; Šijački-Žeravčić, V.; Rajicic, B.; Sedmak, A.; Wasim, M.; Perišić, J. The synergistic action of HELP and HEDE mechanisms of hydrogen embrittlement in steels. In Proceedings of the International Symposium: HYDROGENIUS, I2CNER and HydroMate Joint Research Symposium on HydrogenMaterials Interactions, Fukuoka, Japan, 28–29 January 2021.
9. Liu, J.; Zhao, M.; Rong, L. Overview of hydrogen-resistant alloys for high-pressure hydrogen environment: On the hydrogen energy structural materials. *Clean Energy* **2023**, *7*, 99–115. [CrossRef]
10. Oesterlin, H.; Michler, T.; Fischer, C.; Schönborn, S. Low cycle fatigue testing in high pressure gaseous hydrogen using tubular specimens. In Proceedings of the International Hydrogen Conference: Understanding Hydrogen-Materials Interactions, Park City, UT, USA, 17–21 September 2023.
11. Karniadakis, G.E.; Kevrekidis, I.G.; Lu, L.; Perdikaris, P.; Wang, S.; Yang, L. Physics-informed machine learning. *Nat. Rev. Phys.* **2021**, *3*, 422–440. [CrossRef]
12. Djukic, M.B.; Bakic, G.M.; Sijacki Zeravcic, V.; Sedmak, A.; Rajicic, B. The synergistic action and interplay of hydrogen embrittlement mechanisms in steels and iron: Localized plasticity and decohesion. *Eng. Fract. Mech.* **2019**, *216*, 106528. [CrossRef]
13. Dwivedi, S.K.; Vishwakarma, M. Hydrogen embrittlement in different materials: A review. *Int. J. Hydrog. Energy* **2018**, *43*, 21603–21616. [CrossRef]
14. Correia, J.A.F.O.; Haselibozchaloee, D.; Zhu, S.-P. A review on fatigue design of offshore structures. *Int. J. Ocean. Syst. Manag.* **2025**, *2*, 1–18. [CrossRef]
15. Meng, D.; Yang, S.; Yang, H.; De Jesus, A.M.P.; Correia, J.; Zhu, S.-P. Intelligent-inspired framework for fatigue reliability evaluation of offshore wind turbine support structures under hybrid uncertainty. *Ocean. Eng.* **2024**, *307*, 118213. [CrossRef]
16. Wang, L.; Zhu, S.P.; Luo, C.; Niu, X.; He, J.C. Defect driven physics-informed neural network framework for fatigue life prediction of additively manufactured materials. *Philos. Trans. R. Soc. A* **2023**, *381*, 20220386. [CrossRef]
17. Zhang, Y.; Ai, Y.; Zhang, W. Physics informed ensemble learning used for interval prediction of fracture toughness of pipeline steels in hydrogen environments. *Theor. Appl. Fract. Mech.* **2024**, *130*, 104302. [CrossRef]
18. Abiria, I.; Wang, C.; Zhang, Q.; Liu, C.; Jin, X. High-cycle and very-high-cycle fatigue life prediction in additive manufacturing using hybrid physics-informed neural networks. *Eng. Fract. Mech.* **2025**, *319*, 111026. [CrossRef]

19. Guo, C.; Liu, S.; Gu, T.; Zhou, L.; Zhao, D.; Dong, L.; Zhang, Q.; Wang, Q.; Ling, C. Coupled effects of hydrogen embrittlement and temperature and surface roughness on the mechanical properties of GS80A steel. *Eng. Fail. Anal.* **2024**, *160*, 108112. [CrossRef]
20. Campari, A.; Konert, F.; Razavi, N.; Sobol, O.; Alvaro, A. Hydrogen-assisted cracking: A deep learning approach for fractographic analysis. *Comput. Mater. Sci.* **2026**, *262*, 114366. [CrossRef]
21. Chen, Y.-S.; Huang, C.; Liu, P.-Y.; Yen, H.-W.; Niu, R.; Burr, P.; Moore, K.L.; Martínez-Pañeda, E.; Atrens, A.; Cairney, J.M. Hydrogen trapping and embrittlement in metals—A review. *Int. J. Hydrog. Energy* **2025**, *136*, 789–821. [CrossRef]
22. Hasanli, V. Quantifying conservatism in ASME B31.12 Option A for hydrogen pipeline repurposing. *Int. J. Hydrog. Energy* **2025**, *191*, 103226. [CrossRef]
23. Zelmati, D.; Elsafty, S.; Ostadan, F. Advanced statistical and reliability analysis for corrosion-fatigue performance of hydrogen-impacted pipeline steels. *Reliab. Eng. Syst. Saf.* **2025**, *264*, 111387. [CrossRef]
24. Barrera, O.; Bombac, D.; Chen, Y.; Daff, T.D.; Galindo-Nava, E.; Gong, P.; Haley, D.; Horton, R.; Katzarov, I.; Kermode, J.R.; et al. Understanding and mitigating hydrogen embrittlement of steels: A review of experimental, modelling and characterization progress. *Int. Mater. Rev.* **2018**, *63*, 458–509.
25. Meng, D.; Yang, S.; de Jesus, A.M.P.; Zhu, S.-P. A novel Kriging-model-assisted reliability-based multidisciplinary design optimization strategy and its application in the offshore wind turbine tower. *Renew. Energy* **2023**, *203*, 407–420. [CrossRef]
26. Meng, D.; Yang, H.; Yang, S.; Zhang, Y.; De Jesus, A.M.P.; Correia, J.; Fazeres-Ferradosa, T.; Macek, W.; Branco, R.; Zhu, S.-P. Kriging-assisted hybrid reliability design and optimization of offshore wind turbine support structure based on a portfolio allocation strategy. *Ocean. Eng.* **2024**, *295*, 116842. [CrossRef]
27. Meng, D.; Yang, H.; Fazeres-Ferradosa, T.; Guo, Y.; Khan, M.D.; Zhu, S.-P. Time-varying mesh stiffness modelling of offshore wind gearboxes under multi-fault modes. *Marit. Eng.* **2025**, *178*, 170–195. [CrossRef]
28. Yang, S.; Chen, Y. Modelling and analysis of offshore wind turbine gearbox under multi-field coupling. *Int. J. Ocean. Syst. Manag.* **2025**, *2*, 52–66. [CrossRef]
29. Song, L.K.; Tao, F.; Peng, G.Z. Mixed loss-guided modular regression for dependent system reliability. *Reliab. Eng. Syst. Saf.* **2026**, *267*, 111898. [CrossRef]
30. Song, L.K.; Tao, F.; Choy, Y.; Yang, L.C.; Wei, Y.F. Cascade sampling-driven block mapping for coupled reliability evaluation of turbine cooling systems. *Mech. Syst. Signal Process.* **2025**, *236*, 113008. [CrossRef]
31. Ma, H.; Ma, C.; Xia, W. A method for extracting bearing degradation data of ship propulsion systems based on cumulative features. *Int. J. Ocean. Syst. Manag.* **2025**, *2*, 127–152. [CrossRef]
32. Huang, J.; Ai, Q. Key vulnerability parameters for steel pipe pile-supported wharves considering the uncertainties in structural design. *Int. J. Ocean. Syst. Manag.* **2025**, *2*, 35–51. [CrossRef]
33. Meng, D.; Yang, S.; De Jesus, A.M.P.; Fazeres-Ferradosa, T.; Zhu, S.-P. A novel hybrid adaptive Kriging and water cycle algorithm for reliability-based design and optimization strategy: Application in offshore wind turbine monopile. *Comput. Methods Appl. Mech. Eng.* **2023**, *412*, 116083. [CrossRef]
34. Wang, H.; Zhang, J.; Li, B.; Xuan, F. Machine learning-based fatigue life prediction of laser powder bed fusion additively manufactured Hastelloy X via nondestructively detected defects. *Int. J. Struct. Integr.* **2025**, *16*, 104–126. [CrossRef]
35. Dang, L.; He, X.; Tang, D.; Xin, H.; Wu, B. A fatigue life prediction framework of laser-directed energy deposition Ti-6Al-4V based on physics-informed neural network. *Int. J. Struct. Integr.* **2025**, *16*, 327–354. [CrossRef]
36. Wu, S.; Liu, J.; Wang, Y.; Lu, J.; Zhang, Z. Multiaxial low-cycle fatigue life model for notched specimens considering small sample characteristics. *Int. J. Struct. Integr.* **2024**, *15*, 948–973. [CrossRef]
37. Honarjoo, A.; Darvishan, E.; Rezazadeh, H.; Kosarieh, A.H. SigBERT: Vibration-based steel frame structural damage detection through fine-tuning BERT. *Int. J. Struct. Integr.* **2024**, *15*, 851–872. [CrossRef]
38. Yuan, X.; Li, D.; Wu, H.; Jiang, C. A critical review of machine learning in fatigue life prediction. *Int. J. Fatigue* **2023**, *170*, 107519.
39. Yi, M.; Xue, M.; Cong, P.; Song, Y.; Zhang, H.; Wang, L.; Zhou, L.; Li, Y.; Guo, W. Machine learning for predicting fatigue properties of additively manufactured materials. *Chin. J. Aeronaut.* **2024**, *37*, 1–22. [CrossRef]
40. Luo, X.-L.; Lyu, C.-C.; Zhang, L.-W. Physics-informed ensemble learning for robust extrapolating and revealing fatigue life of composites. *Compos. Sci. Technol.* **2025**, *271*, 111302. [CrossRef]
41. Srinivasan, D.V.; Moradi, M.; Komninos, P.; Zarouchas, D.; Vassilopoulos, A.P. A generalized machine learning framework to estimate fatigue life across materials with minimal data. *Mater. Des.* **2024**, *246*, 113355. [CrossRef]
42. Chen, D.; Li, Y.; Liu, K.; Li, Y. A physics-informed neural network approach to fatigue life prediction using small quantity of samples. *Int. J. Fatigue* **2023**, *166*, 107270. [CrossRef]
43. Song, Y.; Zhang, A. From black box to physically interpretable: Trustworthy computing for AI-driven decision-making and control. *J. Autom. Intell.* **2025**. [CrossRef]
44. El Mir, H.; Perinpanayagam, S. Certification of machine learning algorithms for safe-life assessment of landing gear. *Front. Astron. Space Sci.* **2022**, *9*, 896877. [CrossRef]

45. Yang, S.; Meng, D.; Wang, H.; Yang, C. A novel learning function for adaptive surrogate-model-based reliability evaluation. *Philos. Trans. R. Soc. A-Math. Phys. Eng. Sci.* **2024**, *382*, 20220395. [CrossRef] [PubMed]
46. Song, L.K.; Tao, F.; Li, X.Q.; Yang, L.C.; Wei, Y.P.; Beer, M. Physics-embedding multi-response regressor for time-variant system reliability assessment. *Reliab. Eng. Syst. Saf.* **2025**, *263*, 111262. [CrossRef]
47. Wang, B.; Zhang, P.; Xiang, Y.; Wang, D.; Wu, B.; Wang, X.; Tang, K.; Chen, A. Advancing structural failure analysis with physics-informed machine learning in engineering applications. *Engineering* **2025**. [CrossRef]
48. Geremia, M.; Marella, T.; Ardalani, E.; Beyramysoltan, S.; Chattoraj, S.; Facco, P.; Barolo, M.; Bezzo, F. On the impact of mechanistic model quality and data availability in hybrid model development. *Comput. Chem. Eng.* **2025**, *206*, 109536. [CrossRef]
49. Zhao, Z.; Wang, Y.; Zhang, W.; Ba, Z.; Sun, L. Physics-informed neural networks in heat transfer-dominated multiphysics systems: A comprehensive review. *Eng. Appl. Artif. Intell.* **2025**, *157*, 111098. [CrossRef]
50. Zhou, T.; Jiang, S.; Han, T.; Zhu, S.-P.; Cai, Y. A physically consistent framework for fatigue life prediction using probabilistic physics-informed neural network. *Int. J. Fatigue* **2023**, *166*, 107234. [CrossRef]
51. Zhou, S.; Henrich, M.; Wei, Z.; Feng, F.; Yang, B.; Münstermann, S. A general physics-informed neural network framework for fatigue life prediction of metallic materials. *Eng. Fract. Mech.* **2025**, *322*, 111136. [CrossRef]
52. Bhardwaj, H.K.; Shukla, M. Corrosion fatigue life prediction of multiple austenitic stainless steel grades in high-temperature, high-pressure water environments using a GA-optimized neural network. *Sci. Rep.* **2025**, *15*, 39526. [CrossRef]
53. Dong, X.; Wang, D.; Thoudden-Sukumar, P.; Tehranchi, A.; Ponge, D.; Sun, B.; Raabe, D. Hydrogen-associated decohesion and localized plasticity in a high-Mn and high-Al two-phase lightweight steel. *Acta Mater.* **2022**, *239*, 118296. [CrossRef]
54. Zhao, L.; Ma, C.; Zhao, A.; Fan, Y.; Li, Z. Hydrogen embrittlement behavior of a commercial QP980 steel. *Metals* **2023**, *13*, 1469. [CrossRef]
55. Ogawa, Y.; Umakoshi, K.; Nakamura, M.; Takakuwa, O.; Matsunaga, H. Hydrogen-assisted, intergranular fatigue crack-growth in ferritic iron: Influences of hydrogen-gas pressure and temperature variation. *Int. J. Fatigue* **2020**, *140*, 105806. [CrossRef]
56. Bharati, M.; Maity, R.; Singh, A.; Paul, S.K. The fatigue crack growth behavior of hydrogenated 9Cr-1Mo steel: An experimental and numerical study. *Fatigue Fract. Eng. Mater. Struct.* **2024**, *47*, 1677–1695. [CrossRef]
57. Ogawa, Y.; Takakuwa, O.; Shibata, A. Overview of gaseous hydrogen-assisted fatigue crack growth in ferritic iron and steels: Bridging micro and macro. *Int. J. Hydrog. Energy* **2025**, *102*, 1507–1529. [CrossRef]
58. Kethamukkala, K.; Potts, S.; Liu, Y. Probabilistic hydrogen-assisted fatigue crack growth under random pressure fluctuations in pipeline steels. *Int. J. Press. Vessel. Pip.* **2024**, *211*, 105293. [CrossRef]
59. Motte, R.; De Waele, W. An overview of estimations for the high-cycle fatigue strength of conventionally manufactured steels based on other mechanical properties. *Metals* **2024**, *14*, 85. [CrossRef]
60. Yang, M.; Gao, C.; Pang, J.; Li, S.; Hu, D.; Li, X.; Zhang, Z. High-cycle fatigue behavior and fatigue strength prediction of differently heat-treated 35CrMo steels. *Metals* **2022**, *12*, 688. [CrossRef]
61. Nazar, S.; Proverbio, E. Modeling of hydrogen-assisted fatigue crack growth in carbon steel pipelines. *Int. J. Hydrog. Energy* **2025**, *138*, 548–558. [CrossRef]
62. Hu, J.; Ma, K.; Zhang, Z.; Zhang, R.; Zheng, J. Machine learning-based prediction of hydrogen-assisted fatigue crack growth rate in Cr–Mo steel. *Int. J. Hydrog. Energy* **2025**, *122*, 1–11. [CrossRef]
63. Guo, C.; Liu, S.; Zou, Y.; Zhao, D.; Cheng, M.; Gu, T.; Liu, Y.; Zhang, Q.; Wang, Q.; Feng, Z. Fatigue properties and life prediction of GS80A steel under the effect of hydrogen-rich environment. *JOM* **2023**, *75*, 1306–1318. [CrossRef]
64. Zhang, Q.; Zhang, W.; Chu, W.; Rong, D.; Yang, Q.; Ma, T.; Zhou, C. Data-assisted physics-informed neural network for predicting fatigue life under various strain ratios and pre-strain effect. *Eng. Fract. Mech.* **2025**, *325*, 111319. [CrossRef]
65. Akbari, E.; Chakherlou, T.N.; Tabrizchi, H.; Mosavi, A. Physics-informed neural networks for multiaxial fatigue life prediction of aluminum alloy. *Comput. Model. Eng. Sci.* **2025**, *145*, 305–325. [CrossRef]
66. Yang, S.; De-Jesus, A.M.P.; Meng, D.; Nie, P.; Darabi, R.; Azinpour, E.; Zhu, S.-P. Very high-cycle fatigue behavior of steel in hydrogen environment: State of the art review and challenges. *Eng. Fail. Anal.* **2024**, *166*, 108898. [CrossRef]
67. Saxena, A.; Findley, K.O. A model to account for the effects of load ratio and hydrogen pressure on the fatigue crack growth behavior of pressure vessel steels. *Materials* **2024**, *17*, 4308. [CrossRef]
68. Zeng, B.; Wei, X.-F.; Tan, J.-Z.; Zhang, K.-S. Low cycle fatigue life prediction for hydrogen-charged HRB400 steel based on CPFEM. *Materials* **2025**, *18*, 3920. [CrossRef]

Disclaimer/Publisher's Note: The statements, opinions and data contained in all publications are solely those of the individual author(s) and contributor(s) and not of MDPI and/or the editor(s). MDPI and/or the editor(s) disclaim responsibility for any injury to people or property resulting from any ideas, methods, instructions or products referred to in the content.